SOI: 1.1/TAS DOI: 10.15863/TAS

International Scientific Journal

Theoretical & Applied Science

p-ISSN: 2308-4944 (print) **e-ISSN:** 2409-0085 (online)

Year: 2023 **Issue:** 05 **Volume:** 121

Published: 26.05.2023 **http://T-Science.org**

Issue

Article

Denis Chemezov
Vladimir Industrial College
M.Sc.Eng., Academician of International Academy of
Theoretical and Applied Sciences, Lecturer, Russian Federation
https://orcid.org/0000-0002-2747-552X
vic-science@yandex.ru

Pavel Balabanov
Vladimir Industrial College
Student, Russian Federation

Sergey Lukashov
Vladimir State University named after Alexander & Nikolay Stoletovs
Institute of Mechanical Engineering & Automobile Transport
Student, Russian Federation

Nikita Afanasyev
Vladimir Industrial College
Student, Russian Federation

Maksim Perov
Vladimir Industrial College
Student, Russian Federation

Denis Kosolapov
Vladimir Industrial College
Student, Russian Federation

Ilya Yakovlev
Vladimir Industrial College
Student, Russian Federation

REFERENCE DATA OF PRESSURE DISTRIBUTION ON THE SURFACES OF AIRFOILS HAVING THE NAMES BEGINNING WITH THE LETTER S (THE FIRST PART)

Abstract: *The results of the computer calculation of air flow around the airfoils having the names beginning with the letter S are presented in the article. The contours of pressure distribution on the surfaces of the airfoils at angles of attack of 0, 15 and -15 degrees in conditions of the subsonic airplane flight speed were obtained.*

Key words: *airfoil, angle of attack, pressure, surface.*

Language: *English*

Citation: Chemezov, D., et al. (2023). Reference data of pressure distribution on the surfaces of airfoils having the names beginning with the letter S (the first part). *ISJ Theoretical & Applied Science, 05 (121)*, 331-383.

Soi: http://s-o-i.org/1.1/TAS-05-121-48 ***Doi***: crossref https://dx.doi.org/10.15863/TAS.2023.05.121.48

Scopus ASCC: *1507.*

Introduction

Creating reference materials that determine the most accurate pressure distribution on the airfoil surfaces is an actual task of the airplane aerodynamics.

Materials and methods

The study of air flow around the airfoils was carried out in a two-dimensional formulation by means of the computer calculation in the *Comsol Multiphysics* program. The airfoils in the cross section were taken as objects of research [1-34]. In this work, the airfoils having the names beginning with the letter *S* were adopted. Air flow around the airfoils was carried out at angles of attack (α) of 0, 15 and -15 degrees. Flight speed of the airplane in each case was subsonic. The airplane flight in the atmosphere was carried out under normal weather conditions. The geometric characteristics of the studied airfoils are presented in the Table 1. The geometric shapes of the airfoils in the cross section are presented in the Table 2.

Table 1. The geometric characteristics of the airfoils.

Airfoil name	Max. thickness	Max. camber	Leading edge radius	Trailing edge thickness
S 4110-084-84,61	8.37% at 28.5% of the chord	3.12% at 49.6% of the chord	0.721%	0.0%
S 5020 2,0/8,7	8.64% at 27.2% of the chord	2.0% at 27.2% of the chord	0.713%	0.0%
S1010	6.02% at 23.3% of the chord	0.0% at 0.0% of the chord	0.5829%	0.0%
S1010 HPV airfoil	6.02% at 23.3% of the chord	0.0% at 0.0% of the chord	0.5829%	0.0%
S1012	12.02% at 37.3% of the chord	0.0% at 0.0% of the chord	1.3034%	0.0%
S1014	16.51% at 42.2% of the chord	0.0% at 0.0% of the chord	1.6896%	0.0%
S1016	17.48% at 41.8% of the chord	0.0% at 0.0% of the chord	1.9806%	0.0%
S1020	15.08% at 35.0% of the chord	5.04% at 50.9% of the chord	1.1514%	0.0%
S1046 17% (Danny Howell)	16.99% at 30.8% of the chord	0.0% at 0.0% of the chord	1.5251%	0.0%
S1048 14% (Danny Howell)	13.97% at 27.0% of the chord	0.0% at 0.0% of the chord	1.0073%	0.0%
S1091	5.05% at 14.9% of the chord	6.06% at 42.5% of the chord	0.859%	0.0%
S1210 12%	11.99% at 23.2% of the chord	7.2% at 51.9% of the chord	1.8006%	0.0%
S1221	12.09% at 22.1% of the chord	5.41% at 49.5% of the chord	-0.1118%	0.006%
S1221 w-o flap	12.1% at 22.1% of the chord	5.39% at 49.5% of the chord	1.014%	0.0%
S1221-4	12.13% at 22.1% of the chord	5.4% at 49.6% of the chord	1.6568%	0.715%
S1223	12.13% at 20.3% of the chord	8.67% at 49.9% of the chord	3.085%	0.0%
S1223 RTL	13.48% at 17.8% of the chord	8.46% at 52.8% of the chord	2.5056%	0.0%
S2027	14.5% at 29.4% of the chord	2.73% at 39.1% of the chord	0.9708%	0.0%
S2027-145-83	14.53% at 30.0% of the chord	2.68% at 30.0% of the chord	1.2417%	0.0%
S2046	9.02% at 28.6% of the chord	2.58% at 54.5% of the chord	0.8007%	0.0%
S2048	8.63% at 35.1% of the chord	1.93% at 55.8% of the chord	0.6087%	0.0%
S2050 8,93%	8.93% at 30.2% of the chord	1.25% at 40.2% of the chord	0.7221%	0.0%
S2055	7.98% at 36.2% of the chord	1.65% at 41.3% of the chord	0.5665%	0.0%
S2060 8%	8.0% at 30.2% of the chord	1.81% at 45.6% of the chord	0.6582%	0.0%
S2062 8%	7.98% at 30.4% of the chord	1.73% at 45.9% of the chord	0.6081%	0.0%
S2091	10.23% at 28.6% of the chord	3.96% at 39.1% of the chord	0.8007%	0.367%
S2091-101-83	10.09% at 28.2% of the chord	3.9% at 38.6% of the chord	0.888%	0.0%
S3002	9.93% at 28.7% of the chord	2.99% at 38.8% of the chord	0.7056%	0.483%
S3010	10.31% at 24.6% of the chord	2.82% at 39.6% of the chord	1.1058%	0.118%
S3010-103-84	10.31% at 24.6% of the chord	2.82% at 39.6% of the chord	1.0337%	0.0%
S3014	9.45% at 30.5% of the chord	2.56% at 40.8% of the chord	0.6837%	0.021%
S3014-095-85	9.45% at 30.5% of the chord	2.56% at 40.8% of the chord	0.7267%	0.0%
S3016	9.53% at 31.0% of the chord	2.09% at 41.2% of the chord	0.8561%	0.029%
S3016-095-87	9.5% at 30.9% of the chord	2.08% at 41.0% of the chord	0.7131%	0.0%
S3021	9.47% at 29.9% of the chord	2.95% at 40.2% of the chord	0.6813%	0.172%
S3021-095-84	9.47% at 29.9% of the chord	2.95% at 40.2% of the chord	0.7081%	0.0%
S3024 9,84%	9.82% at 29.2% of the chord	3.52% at 45.0% of the chord	0.7822%	0.0%
S3025 9,38%	9.37% at 28.9% of the chord	3.59% at 39.2% of the chord	0.7478%	0.0%
S4022	11.24% at 35.7% of the chord	4.34% at 56.9% of the chord	0.6133%	0.0%
S4053	8.91% at 34.7% of the chord	2.99% at 45.3% of the chord	0.5489%	0.0%
S4061	9.74% at 28.7% of the chord	3.96% at 44.7% of the chord	0.5734%	0.363%
S4061-096-84	9.61% at 28.3% of the chord	3.9% at 44.2% of the chord	0.8395%	0.0%
S4062	9.56% at 33.2% of the chord	4.14% at 49.5% of the chord	0.8339%	0.178%
S4062-095-87	9.52% at 33.0% of the chord	4.13% at 49.3% of the chord	0.7083%	0.0%
S4080	8.01% at 28.3% of the chord	2.97% at 39.8% of the chord	0.4994%	0.27%
S4081	8.01% at 28.3% of the chord	2.96% at 39.8% of the chord	0.4655%	0.272%
S4082	8.51% at 24.7% of the chord	3.54% at 36.0% of the chord	0.7527%	0.221%
S4083 (8%)	8.0% at 24.7% of the chord	3.45% at 36.0% of the chord	0.522%	0.0%
S4110	8.37% at 28.5% of the chord	3.12% at 49.6% of the chord	0.6732%	0.055%

S4158	10.85% at 34.6% of the chord	3.7% at 45.2% of the chord	0.7503%	0.0%
S4180	9.87% at 27.8% of the chord	4.42% at 38.4% of the chord	1.4374%	0.376%
S4180-098-84	9.74% at 27.5% of the chord	4.36% at 37.9% of the chord	1.0996%	0.0%
S4233	13.64% at 33.8% of the chord	3.26% at 44.0% of the chord	0.6194%	0.461%
S4233-136-84	13.64% at 33.8% of the chord	3.26% at 44.0% of the chord	0.9901%	0.0%
S4310	10.83% at 28.4% of the chord	4.15% at 38.7% of the chord	0.8353%	0.0%
S4320	9.4% at 27.7% of the chord	4.46% at 38.1% of the chord	0.8166%	0.0%
S5010	9.82% at 27.0% of the chord	2.19% at 27.0% of the chord	0.7541%	0.0%
S5010-98	9.85% at 27.1% of the chord	2.2% at 27.1% of the chord	0.7559%	0.02%
S5020	8.39% at 27.2% of the chord	2.61% at 27.2% of the chord	0.6604%	0.0%
S5020-84	8.42% at 27.2% of the chord	2.62% at 27.2% of the chord	0.7362%	0.015%
S6061 9%	9.0% at 31.1% of the chord	1.75% at 41.2% of the chord	0.6096%	0.0%
S6062 8%	7.94% at 31.3% of the chord	1.58% at 41.5% of the chord	0.5654%	0.0%
S6063 7,05%	6.95% at 26.7% of the chord	1.42% at 41.7% of the chord	0.5295%	0.0%
S7012 8,75%	8.74% at 30.1% of the chord	2.02% at 37.6% of the chord	0.4603%	0.0%
S7055 (10,5%) Flat-Bottomed	10.48% at 33.0% of the chord	3.54% at 40.9% of the chord	0.5968%	0.0%
S7075 (9%)	9.0% at 28.7% of the chord	3.02% at 44.3% of the chord	0.6706%	0.0%
S8025 (8%)	7.98% at 22.8% of the chord	0.48% at 16.7% of the chord	0.6528%	0.0%
S8035 for RC aerobatic 14% thick	14.0% at 29.1% of the chord	0.0% at 0.0% of the chord	1.4028%	0.0%
S8035-17,5%	17.5% at 29.1% of the chord	0.0% at 0.0% of the chord	2.1695%	0.0%
S8036 (16%)	15.99% at 34.2% of the chord	1.85% at 34.2% of the chord	1.5975%	0.0%
S8037 (16%)	16.0% at 34.0% of the chord	2.62% at 34.0% of the chord	1.6089%	0.0%
S8038 (13%)	12.99% at 31.1% of the chord	0.89% at 31.1% of the chord	1.0345%	0.0%
S8052 (11,88%)	11.88% at 34.5% of the chord	1.57% at 38.3% of the chord	0.9387%	0.0%
S8055 (12%)	12.0% at 34.3% of the chord	2.04% at 41.9% of the chord	1.0404%	0.0%
SA7035	9.19% at 29.8% of the chord	2.55% at 41.3% of the chord	0.444%	0.0%
SA7036	9.19% at 29.5% of the chord	2.78% at 41.0% of the chord	0.482%	0.0%
SA7038	9.2% at 28.9% of the chord	3.23% at 40.4% of the chord	0.5741%	0.0%
SARATOV	9.2% at 15.0% of the chord	9.75% at 40.0% of the chord	1.2494%	0.0%
SAUTER1	15.0% at 30.0% of the chord	6.55% at 30.0% of the chord	1.9788%	0.154%
SAUTER2	14.0% at 30.0% of the chord	6.34% at 30.0% of the chord	1.7385%	0.144%
SAUTER3	13.5% at 30.0% of the chord	6.23% at 30.0% of the chord	1.6263%	0.138%
SAUTER4	12.5% at 30.0% of the chord	6.02% at 30.0% of the chord	1.4174%	0.128%
SAUTER5	11.0% at 30.0% of the chord	5.7% at 30.0% of the chord	1.1464%	0.113%
SB 96 12.7/3.0	12.55% at 31.4% of the chord	3.09% at 49.7% of the chord	0.8995%	0.0%
SB 97 8/1.25	8.0% at 28.7% of the chord	1.27% at 41.2% of the chord	0.5918%	0.1206%
SB 98 VM5	10.94% at 32.0% of the chord	1.9% at 36.5% of the chord	0.915%	0.0197%
SB 98 VR5	11.97% at 31.2% of the chord	1.92% at 41.1% of the chord	1.3637%	0.14%
SB 98 VS5	9.98% at 33.1% of the chord	1.9% at 37.2% of the chord	0.5779%	0.0402%
SB 99 F3J	8.98% at 30.4% of the chord	3.52% at 39.2% of the chord	0.7283%	0.1356%
SB95 9.5/2	9.54% at 32.4% of the chord	1.94% at 45.8% of the chord	0.8704%	0.2024%
SB95 10.5/2	10.49% at 30.5% of the chord	1.95% at 44.3% of the chord	1.0262%	0.2238%
SB95 11.5/2	11.48% at 32.5% of the chord	1.95% at 42.0% of the chord	1.2523%	0.2452%

Note:
S2027-145-83 (M. Selig (USA));
S8035-17,5% (-Mod.).

Table 2. The geometric shapes of the airfoils in the cross section.

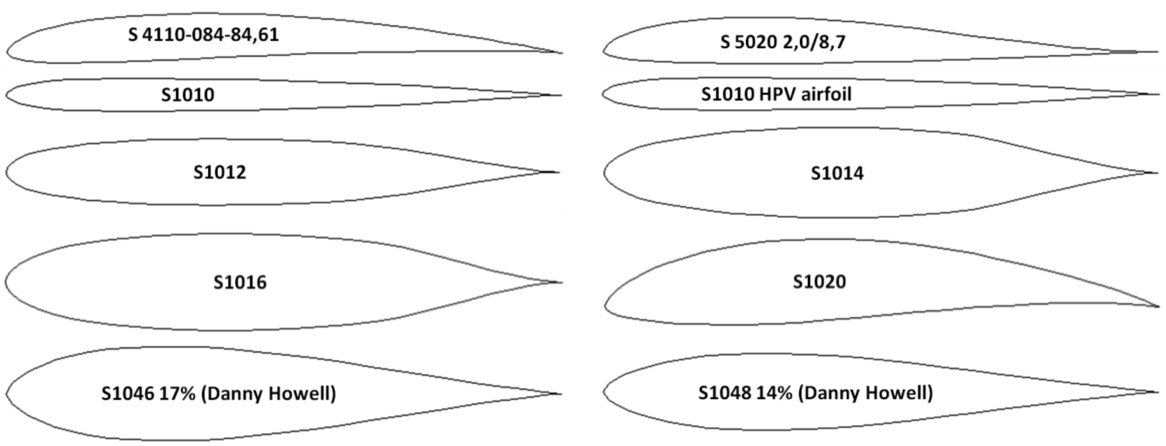

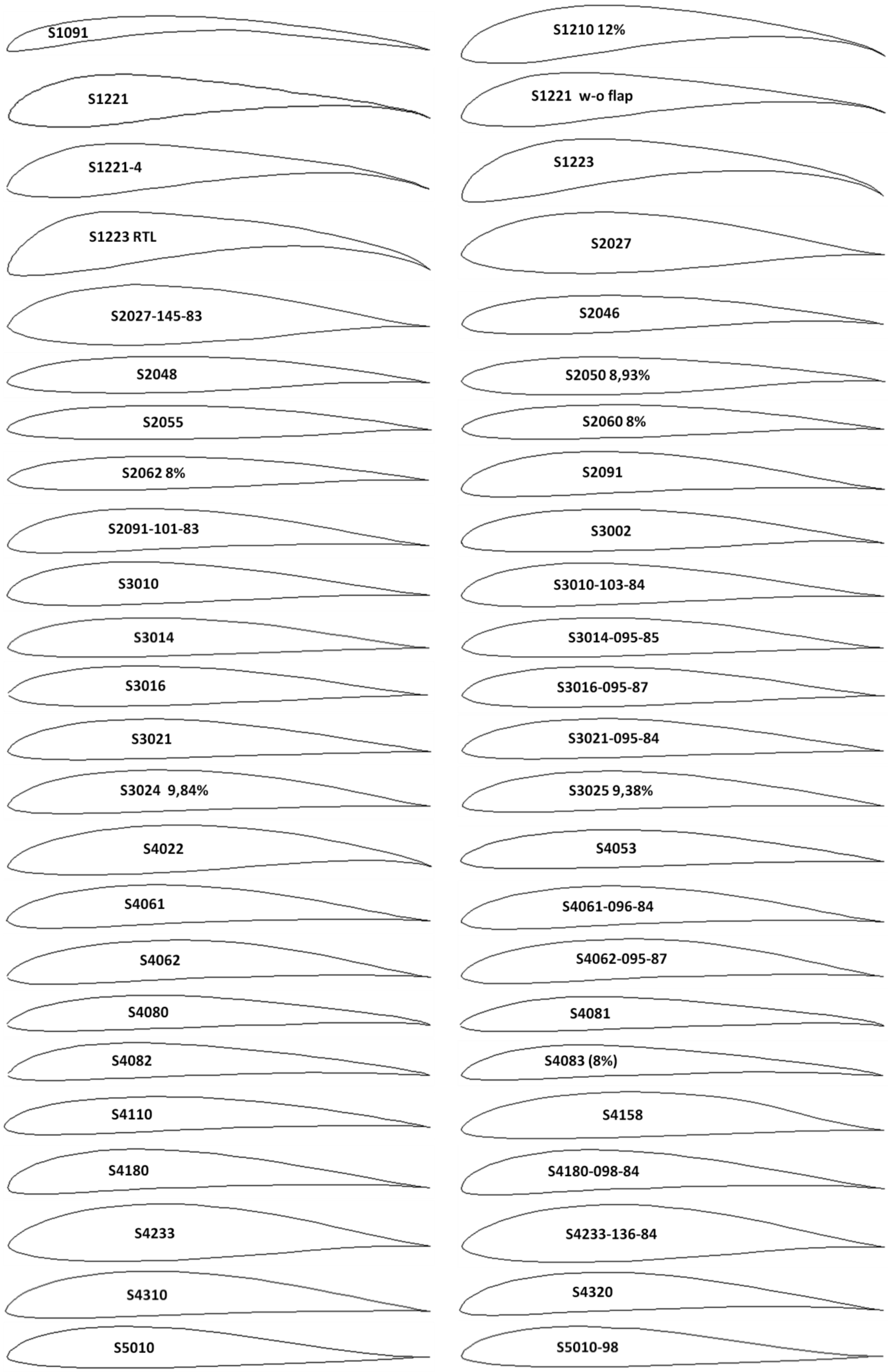

S1091
S1210 12%
S1221
S1221 w-o flap
S1221-4
S1223
S1223 RTL
S2027
S2027-145-83
S2046
S2048
S2050 8,93%
S2055
S2060 8%
S2062 8%
S2091
S2091-101-83
S3002
S3010
S3010-103-84
S3014
S3014-095-85
S3016
S3016-095-87
S3021
S3021-095-84
S3024 9,84%
S3025 9,38%
S4022
S4053
S4061
S4061-096-84
S4062
S4062-095-87
S4080
S4081
S4082
S4083 (8%)
S4110
S4158
S4180
S4180-098-84
S4233
S4233-136-84
S4310
S4320
S5010
S5010-98

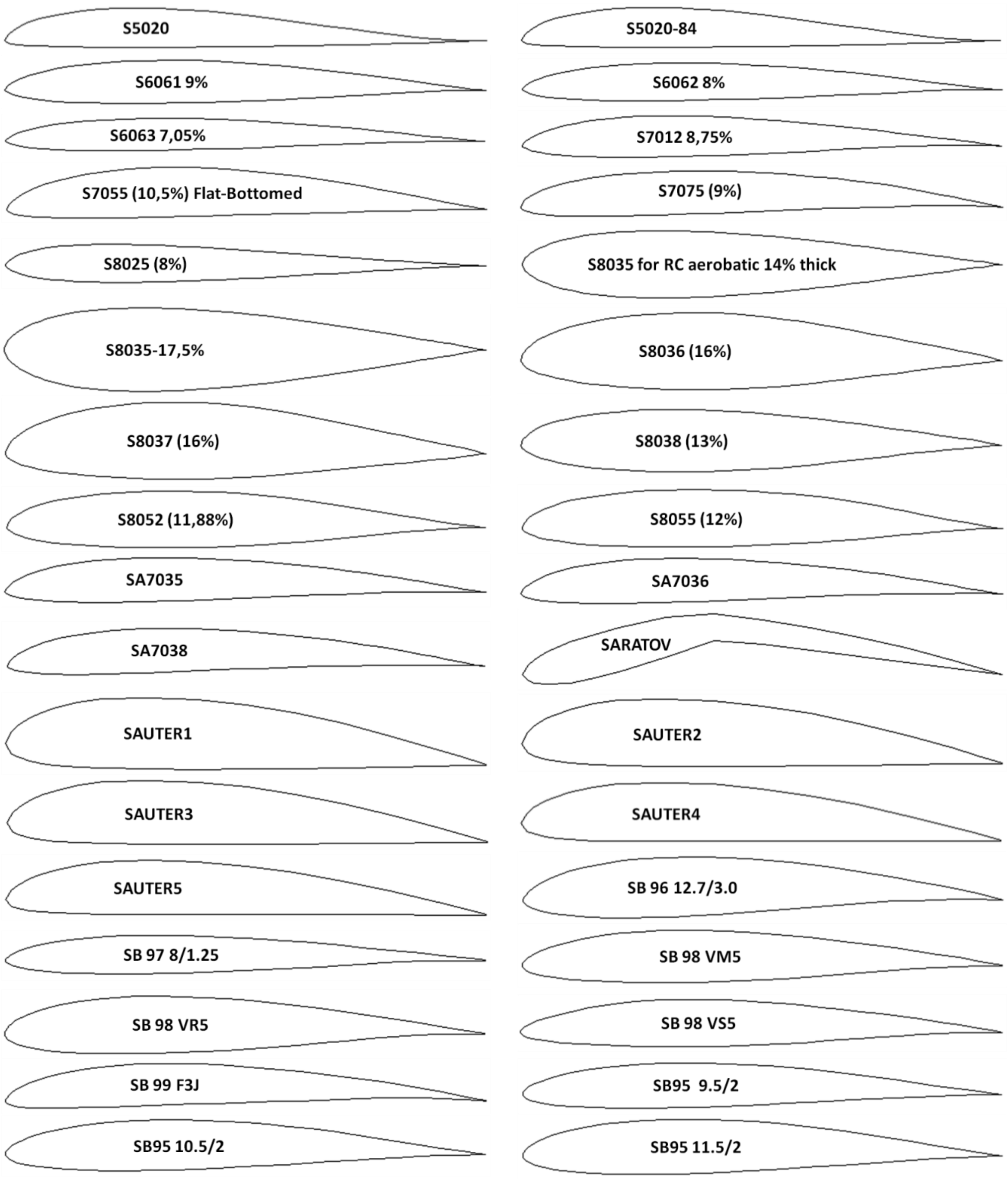

Results and discussion

The calculated pressure contours on the surfaces of the airfoils at different angles of attack are presented in the Figs. 1-92. The calculated values on the scale can be represented as the basic values when comparing the pressure drop under conditions of changing the angle of attack of the airfoils.

92 airfoils of the S, SAUTER, SB and others types were considered in this paper. All airfoils are asymmetrical, with the exception of S1010, S1010 HPV airfoil, S1012, S1014, S1016, S1046 17% (Danny Howell), S1014 14% (Danny Howell), S8035 for RC aerobatic 14% thick and S8035-17,5%. The largest and smallest thicknesses of the studied airfoils are 17.5% and 5.05% for S8035-17.5% and S1091, respectively. The largest and smallest cambers are 9.75% and 0.0% for SARATOV and all symmetrical airfoils, respectively. The largest and smallest leading edge radii are 3.085% and -0.1118% for S1223 and S1221, respectively. The largest and smallest trailing edge thicknesses are 0.715% and 0.0% for S121-4 and for most of the considered airfoils, respectively.

Let us consider in detail the aerodynamic characteristics of some airfoils: S1020, S1223 RTL, S4158, S7055 (10,5%) Flat-Bottomed, S8035 for RC aerobatic 14% thick, SARATOV and SB 98 VS5.

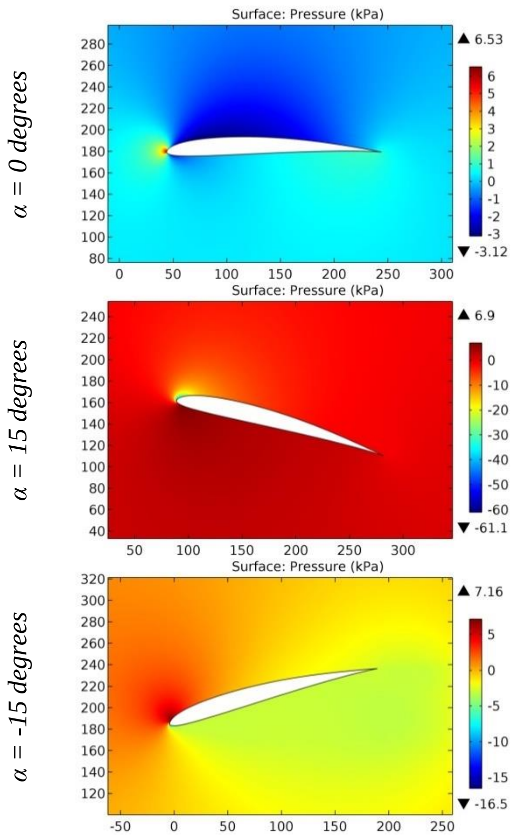

Figure 1. The pressure contours on the surfaces of the S 4110-084-84,61 airfoil.

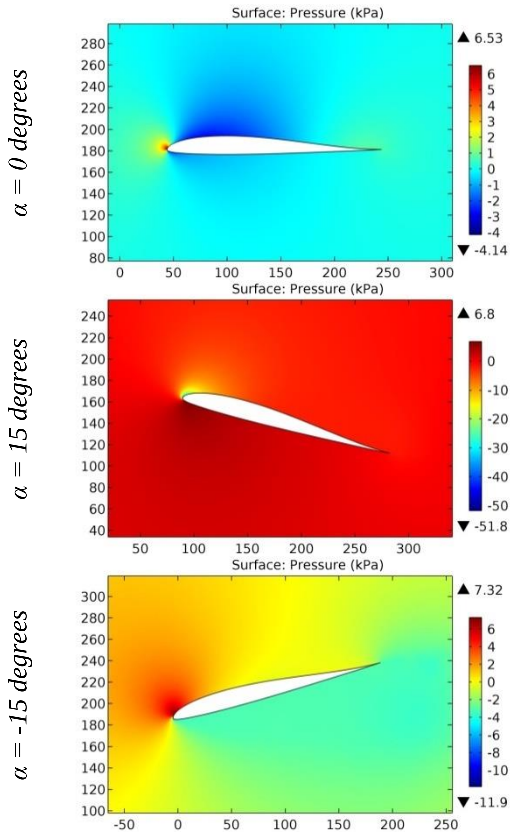

Figure 2. The pressure contours on the surfaces of the S 5020 2,0/8,7 airfoil.

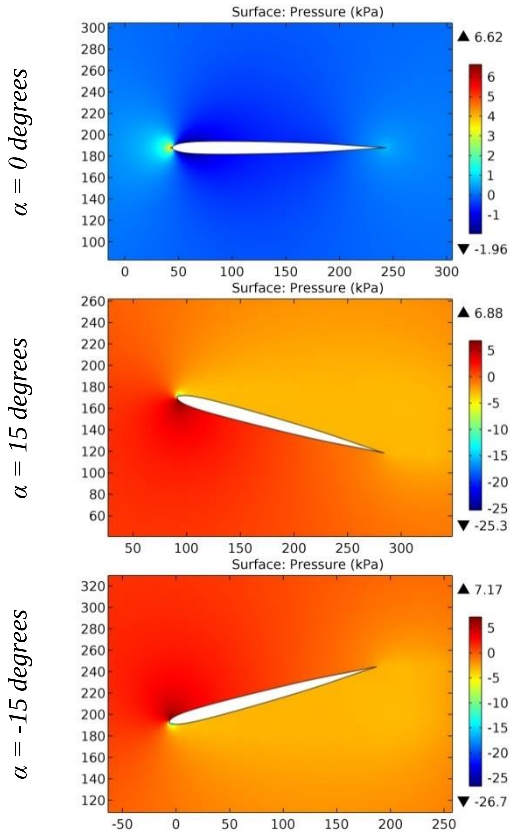

Figure 3. The pressure contours on the surfaces of the S1010 airfoil.

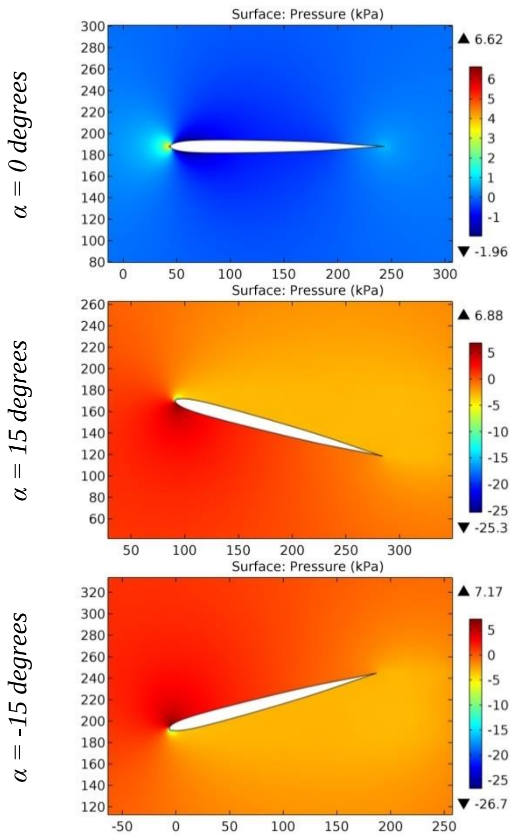

Figure 4. The pressure contours on the surfaces of the S1010 HPV airfoil.

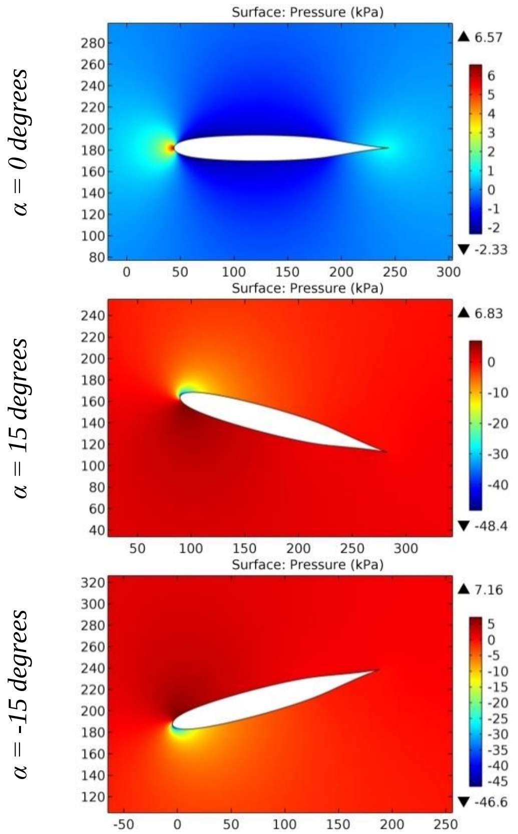

Figure 5. The pressure contours on the surfaces of the S1012 airfoil.

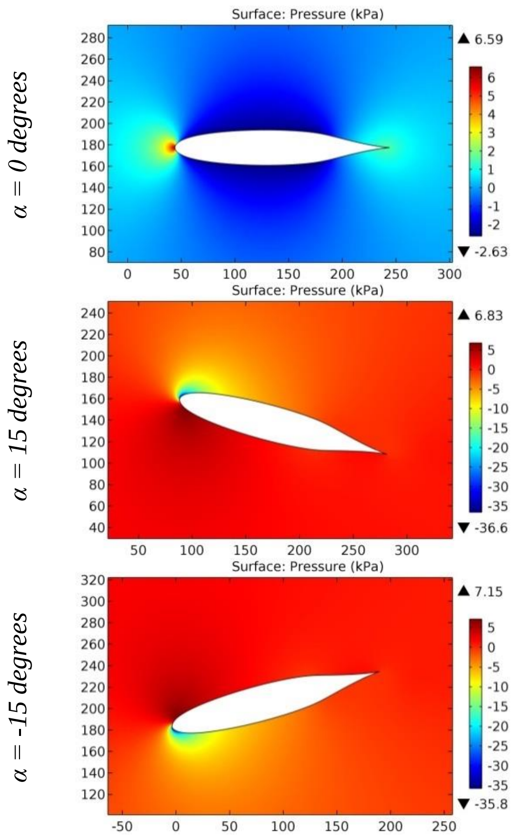

Figure 6. The pressure contours on the surfaces of the S1014 airfoil.

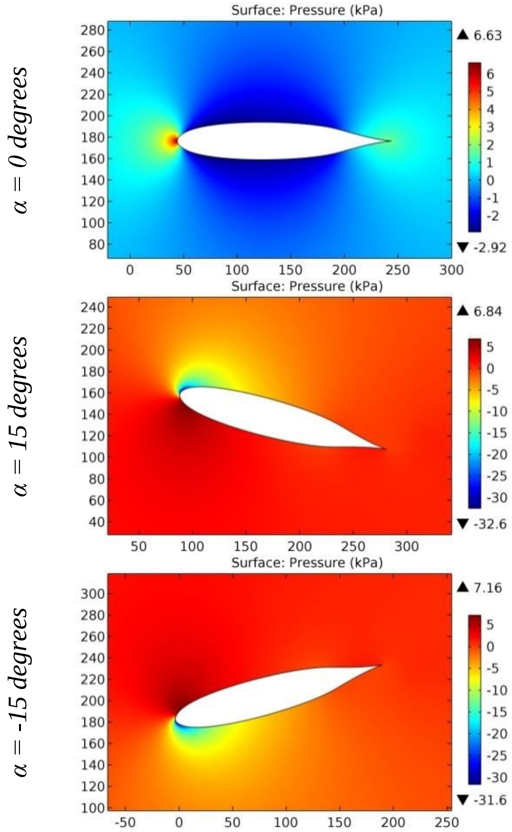

Figure 7. The pressure contours on the surfaces of the S1016 airfoil.

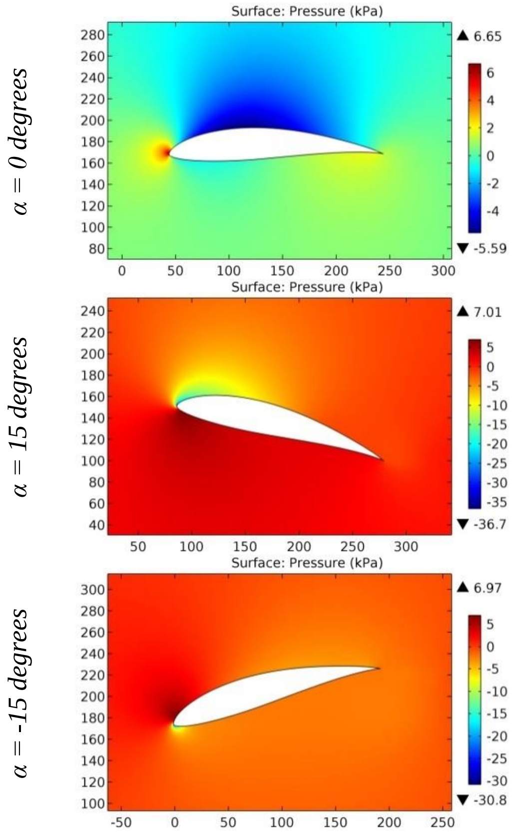

Figure 8. The pressure contours on the surfaces of the S1020 airfoil.

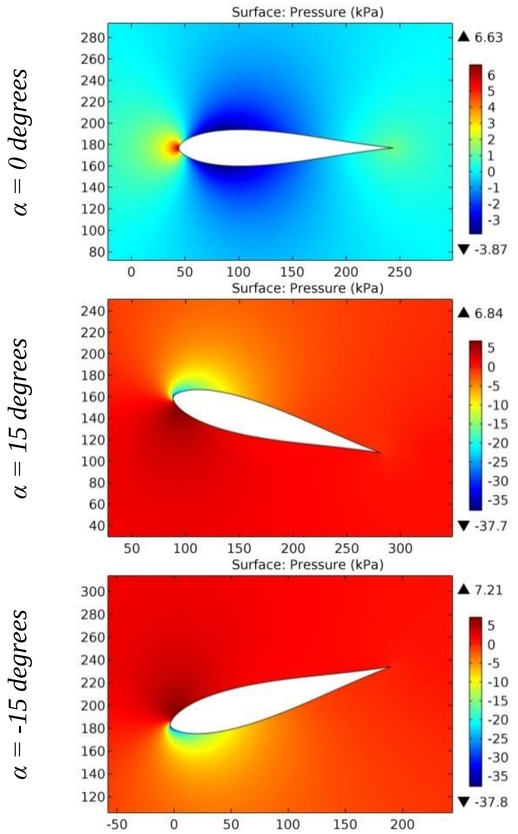

Figure 9. The pressure contours on the surfaces of the S1046 17% (Danny Howell) airfoil.

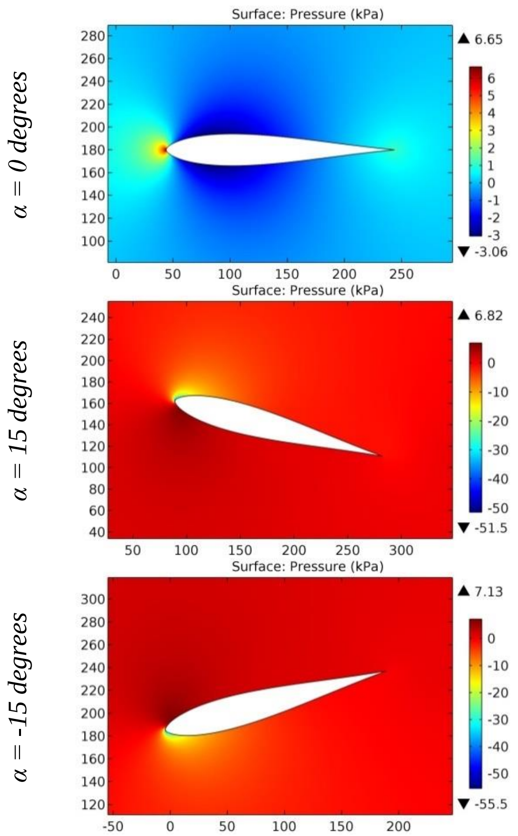

Figure 10. The pressure contours on the surfaces of the S1048 14% (Danny Howell) airfoil.

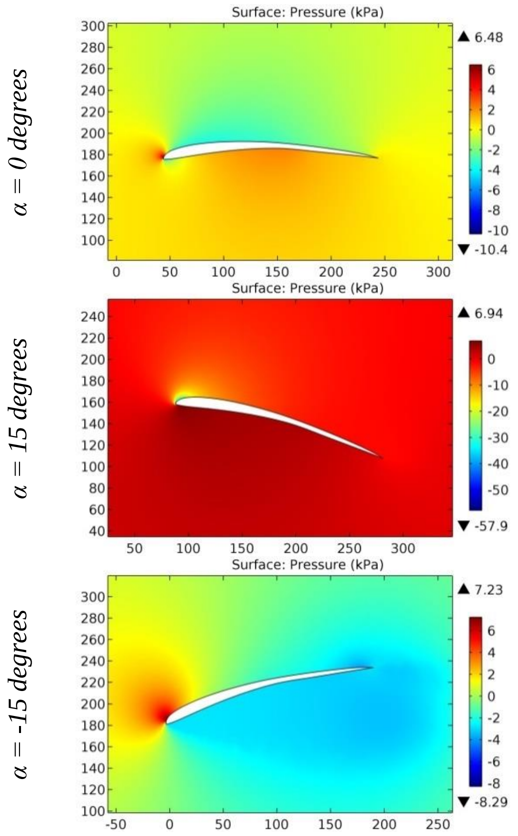

Figure 11. The pressure contours on the surfaces of the S1091 airfoil.

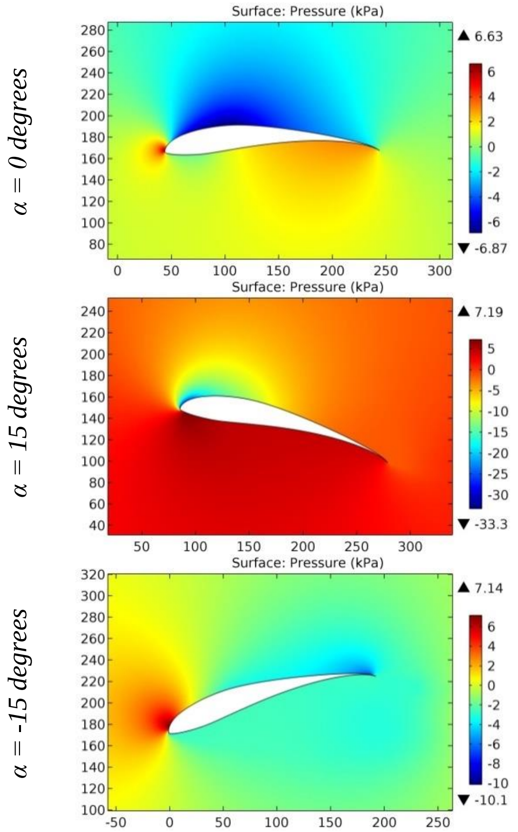

Figure 12. The pressure contours on the surfaces of the S1210 12% airfoil.

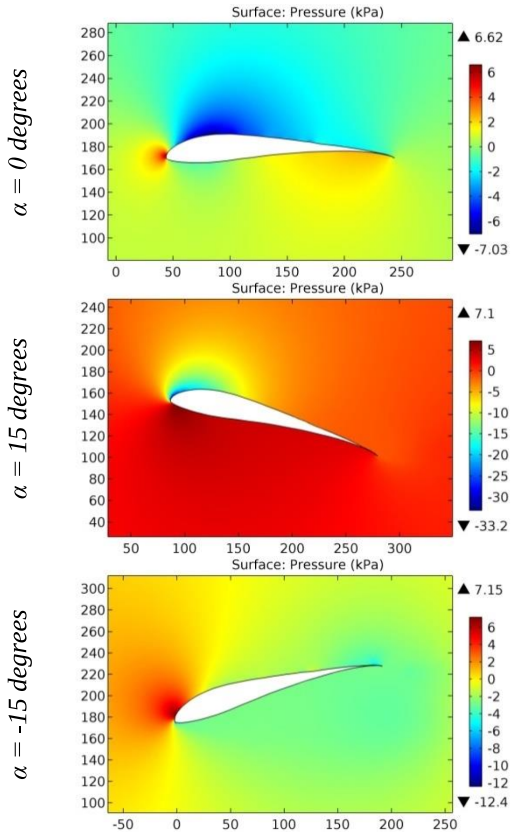

Figure 13. The pressure contours on the surfaces of the S1221 airfoil.

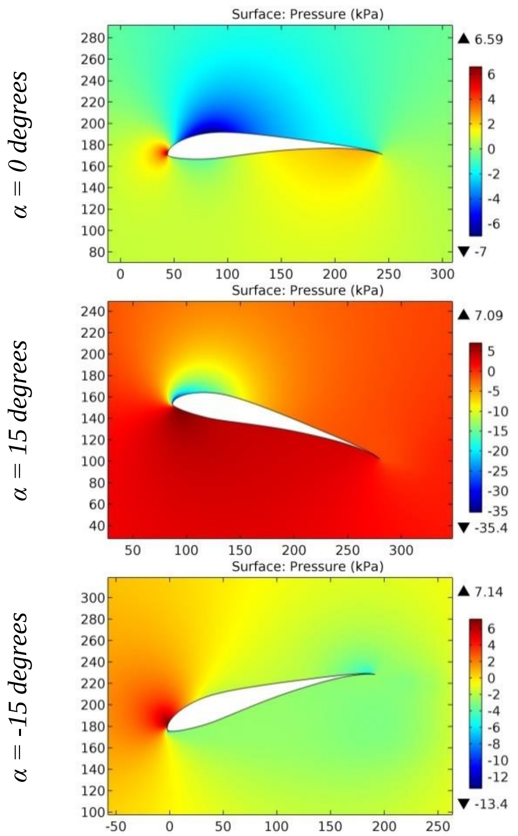

Figure 14. The pressure contours on the surfaces of the S1221 w-o flap airfoil.

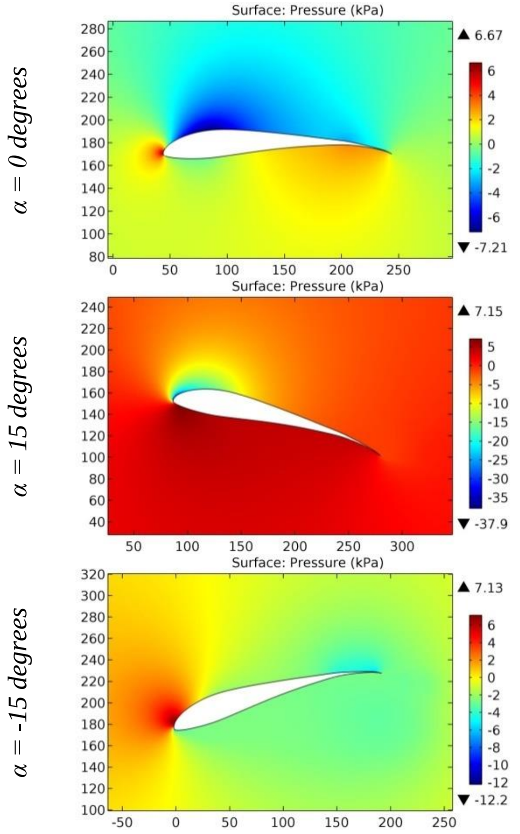

Figure 15. The pressure contours on the surfaces of the S1221-4 airfoil.

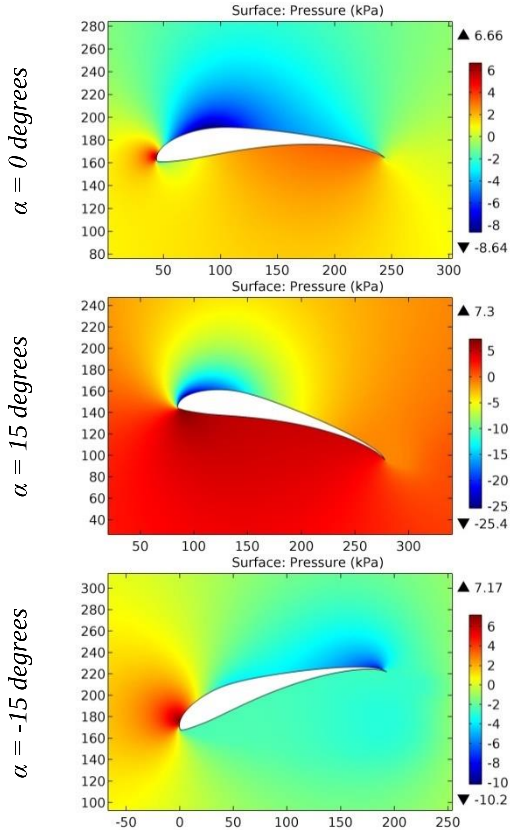

Figure 16. The pressure contours on the surfaces of the S1223 airfoil.

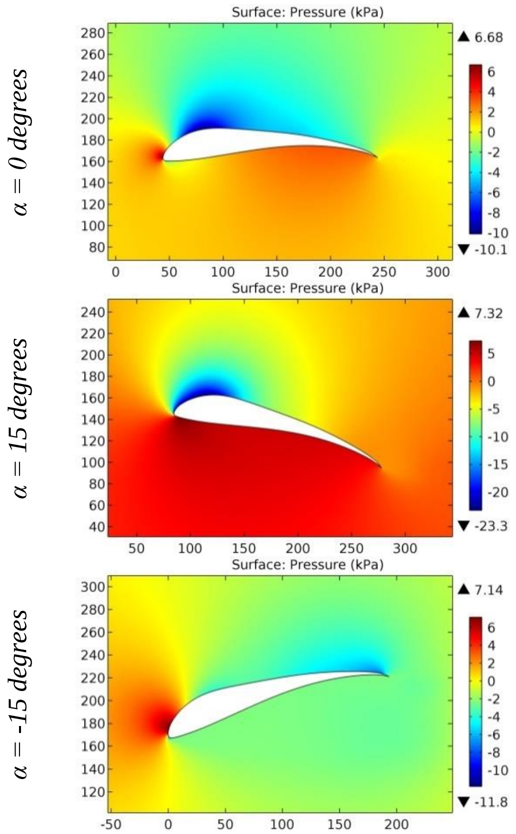

Figure 17. The pressure contours on the surfaces of the S1223 RTL airfoil.

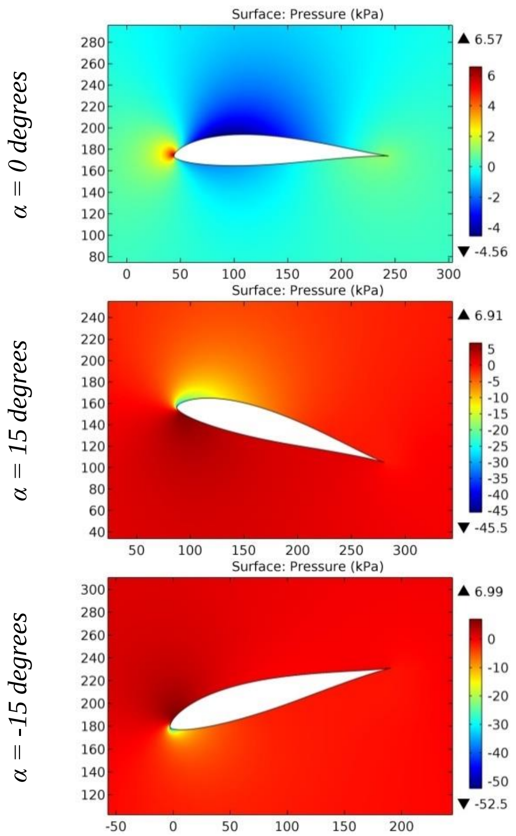

Figure 18. The pressure contours on the surfaces of the S2027 airfoil.

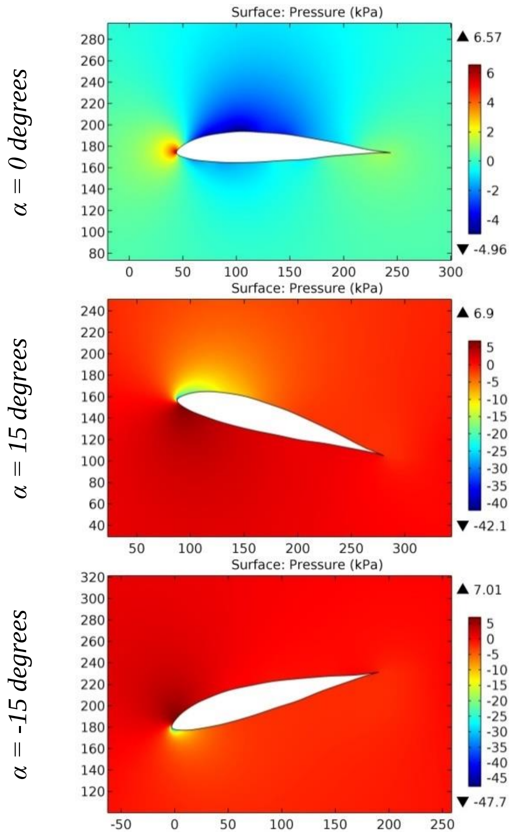

Figure 19. The pressure contours on the surfaces of the S2027-145-83 airfoil.

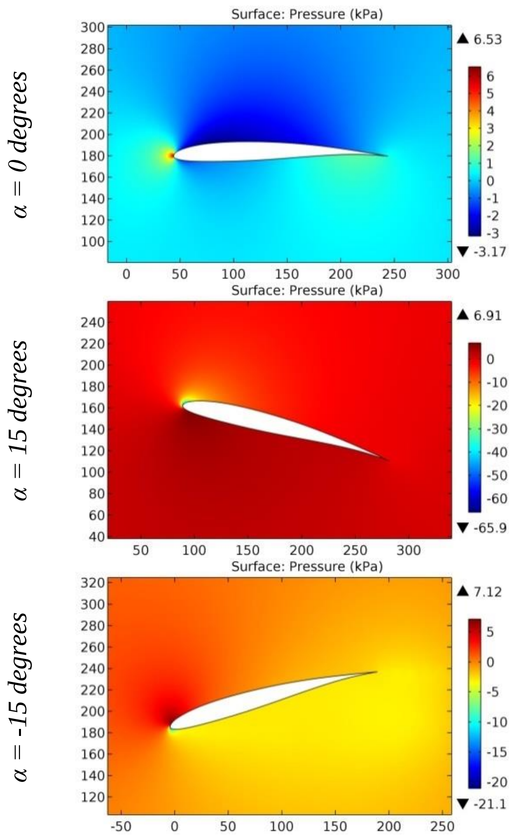

Figure 20. The pressure contours on the surfaces of the S2046 airfoil.

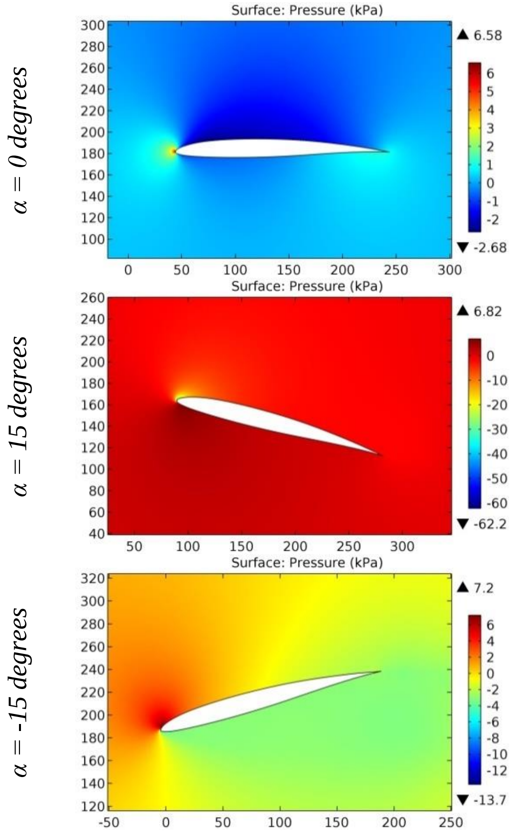

Figure 21. The pressure contours on the surfaces of the S2048 airfoil.

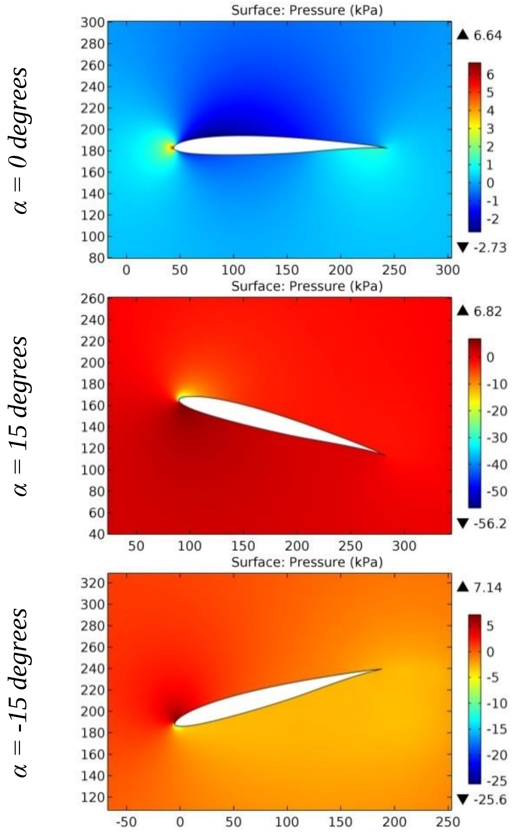

Figure 22. The pressure contours on the surfaces of the S2050 8,93% airfoil.

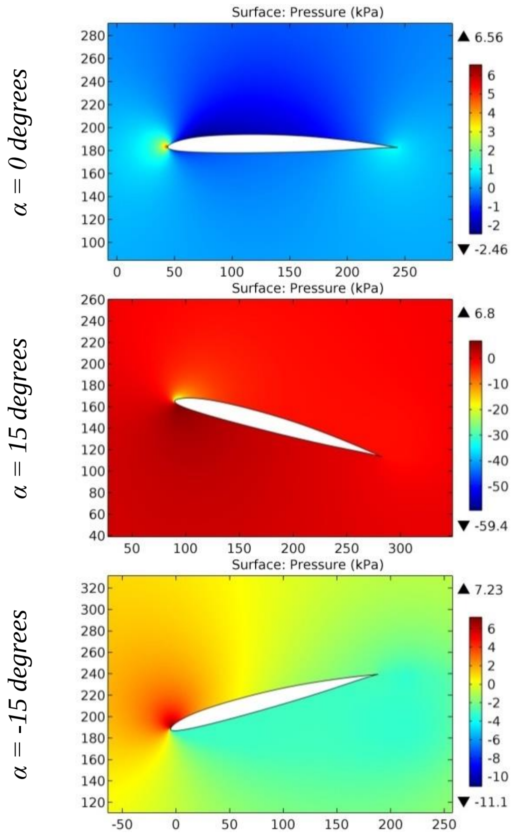

Figure 23. The pressure contours on the surfaces of the S2055 airfoil.

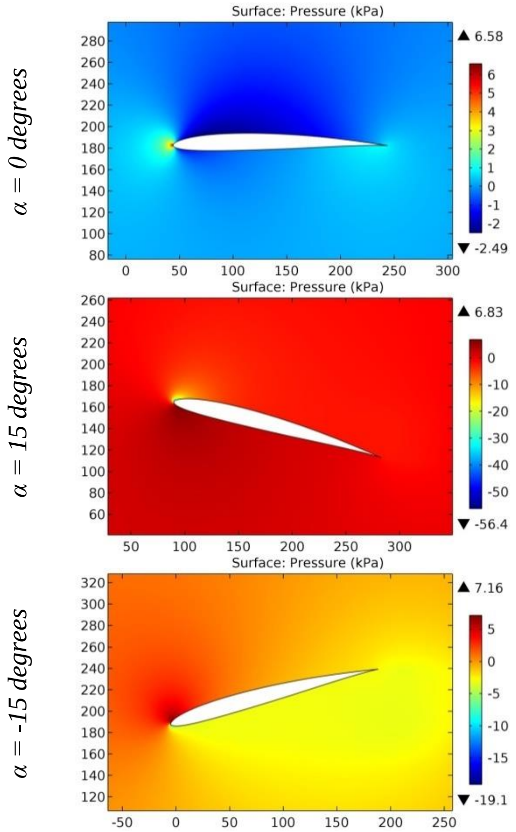

Figure 24. The pressure contours on the surfaces of the S2060 8% airfoil.

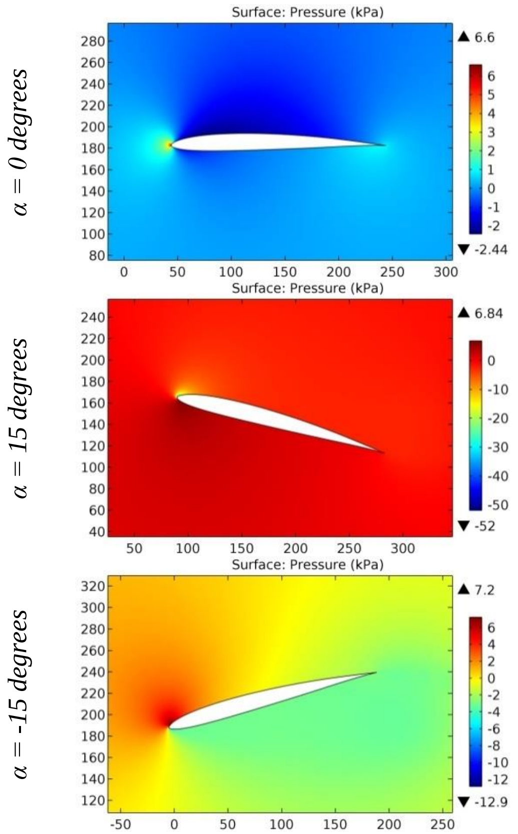

Figure 25. The pressure contours on the surfaces of the S2062 8% airfoil.

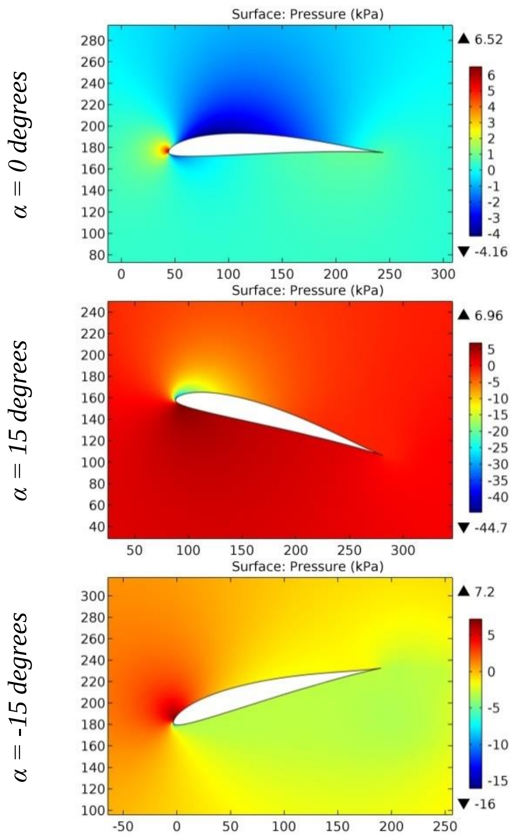

Figure 26. The pressure contours on the surfaces of the S2091 airfoil.

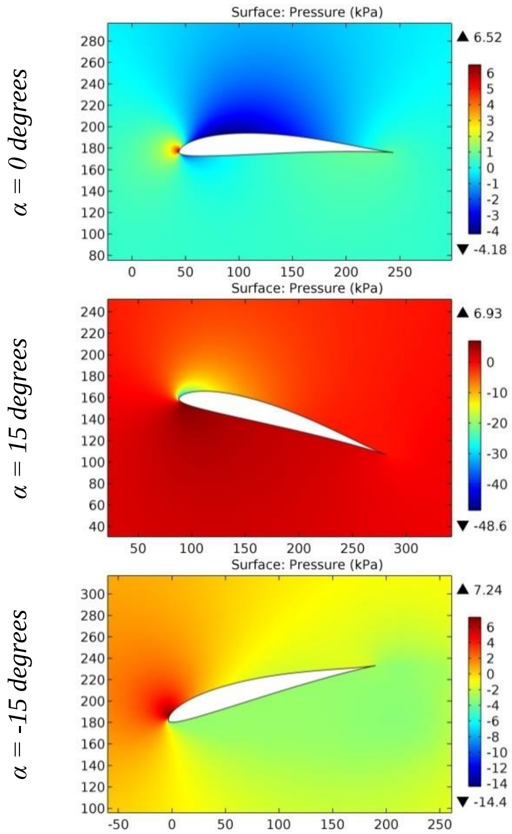

Figure 27. The pressure contours on the surfaces of the S2091-101-83 airfoil.

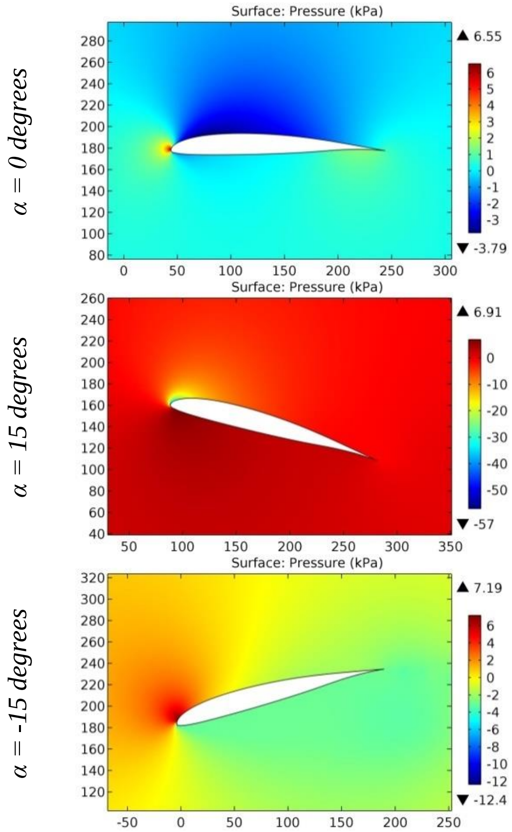

Figure 28. The pressure contours on the surfaces of the S3002 airfoil.

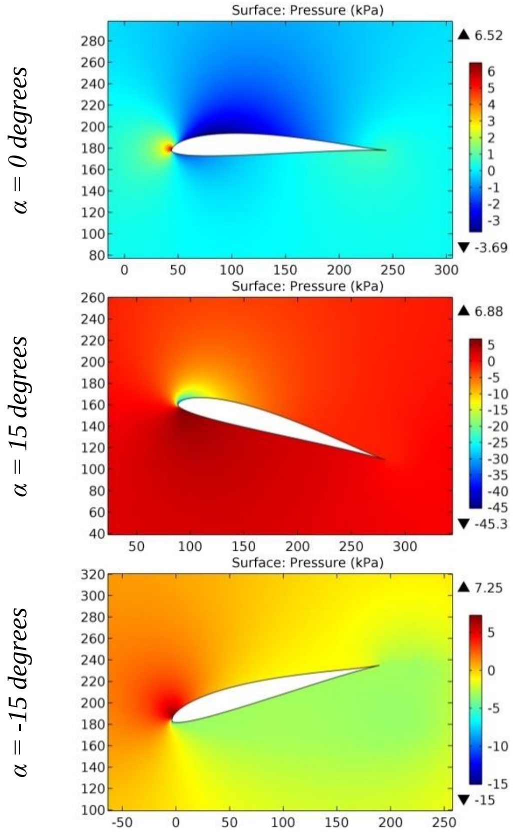

Figure 29. The pressure contours on the surfaces of the S3010 airfoil.

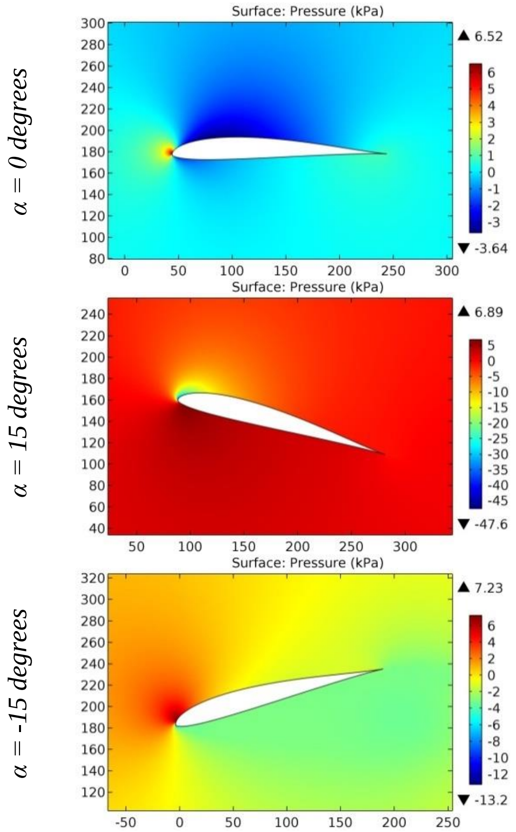

Figure 30. The pressure contours on the surfaces of the S3010-103-84 airfoil.

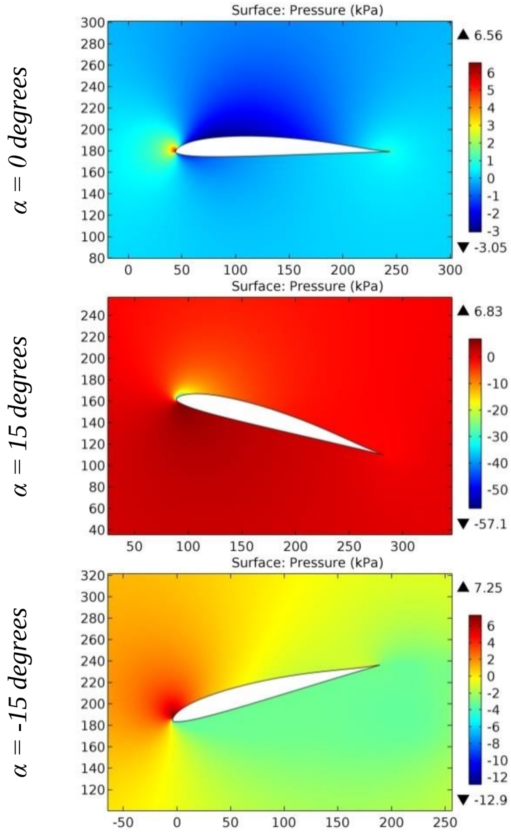

Figure 31. The pressure contours on the surfaces of the S3014 airfoil.

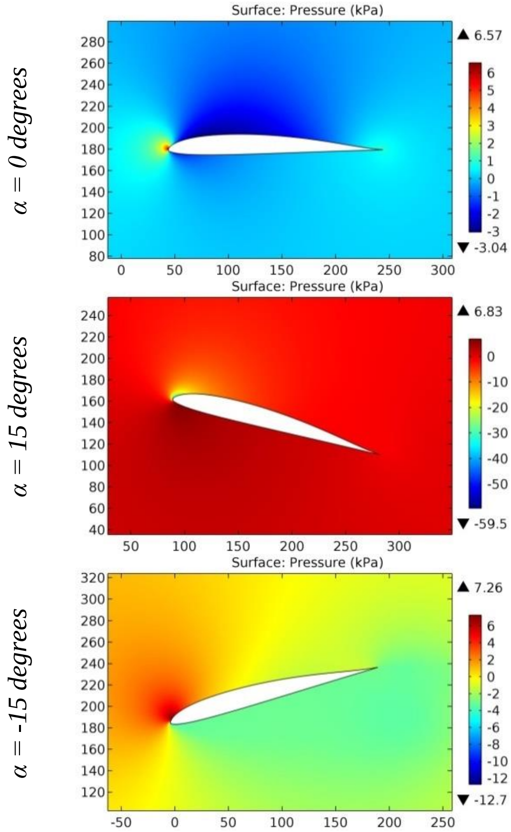

Figure 32. The pressure contours on the surfaces of the S3014-095-85 airfoil.

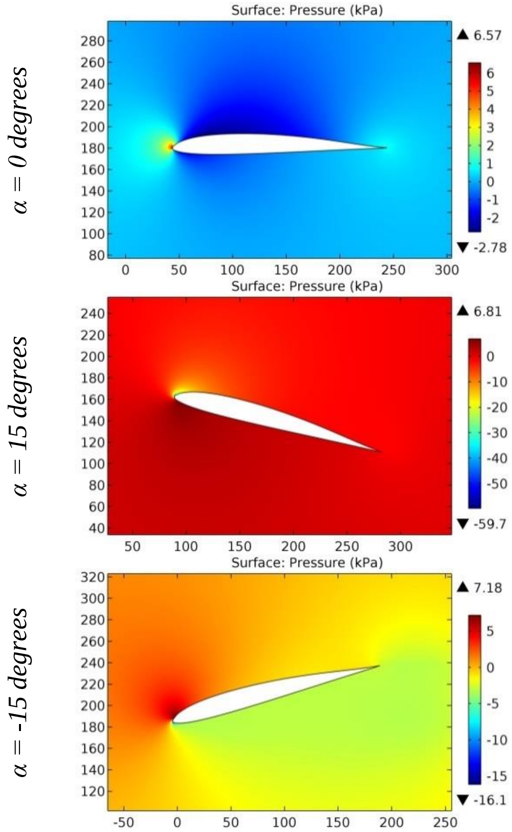

Figure 33. The pressure contours on the surfaces of the S3016 airfoil.

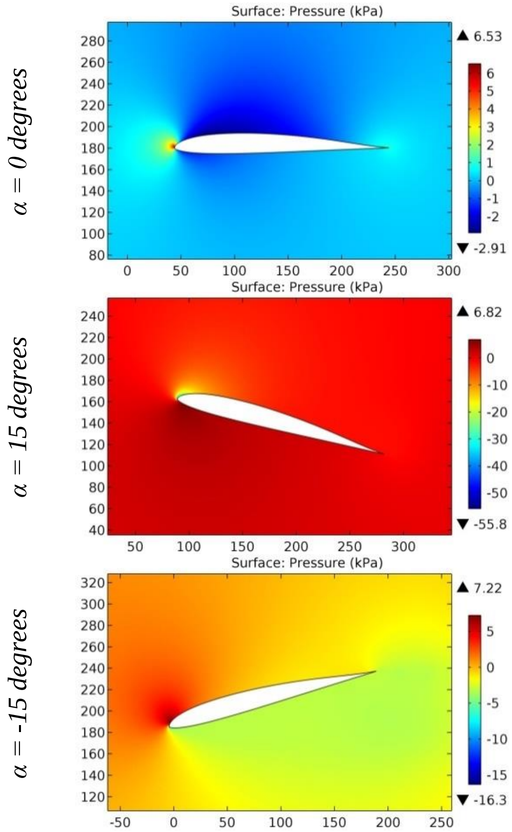

Figure 34. The pressure contours on the surfaces of the S3016-095-87 airfoil.

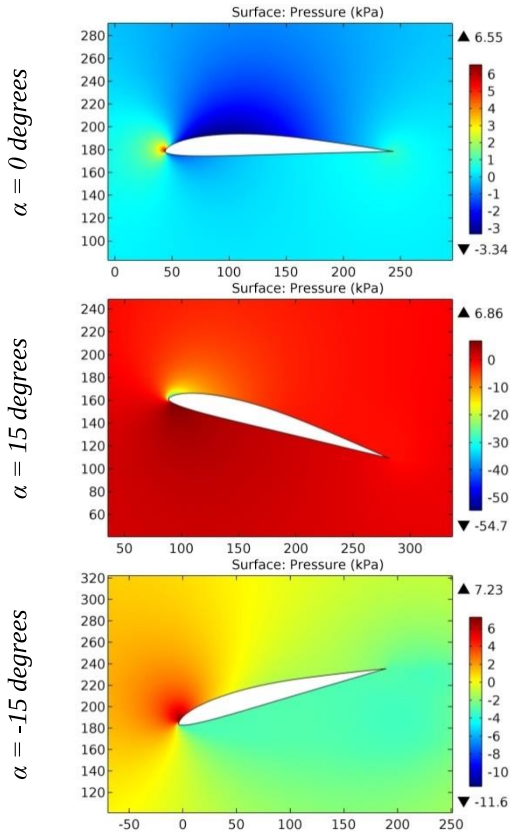

Figure 35. The pressure contours on the surfaces of the S3021 airfoil.

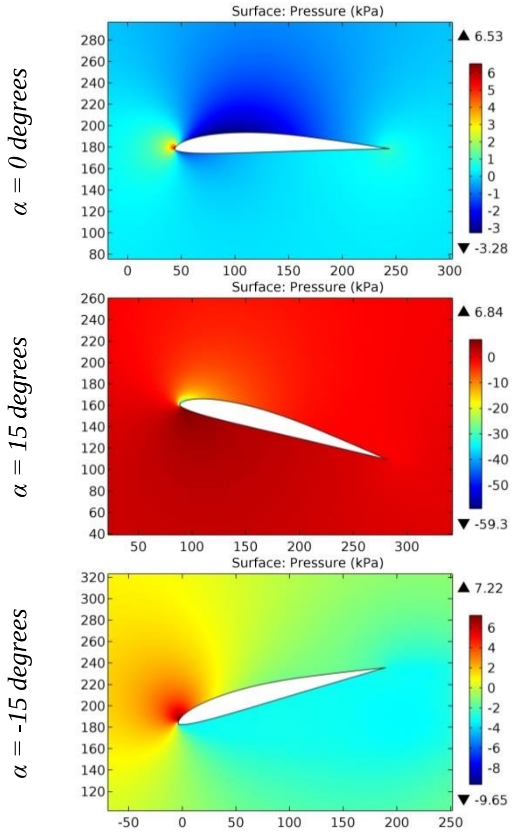

Figure 36. The pressure contours on the surfaces of the S3021-095-84 airfoil.

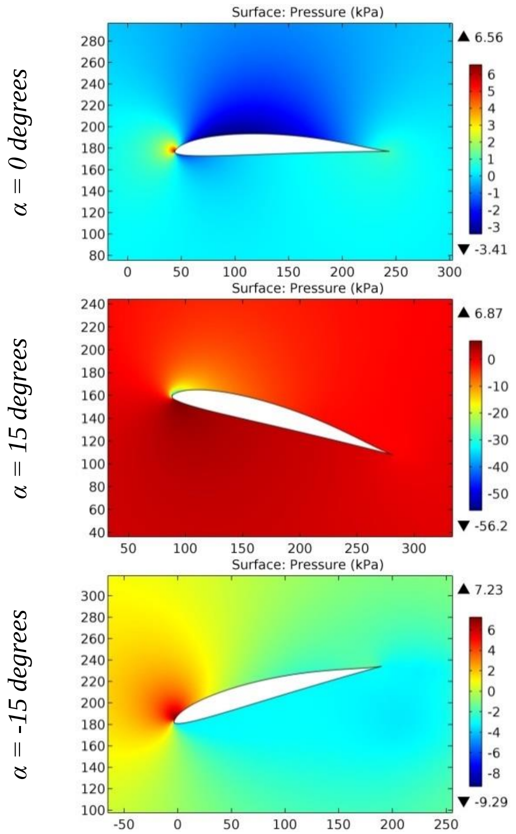

Figure 37. The pressure contours on the surfaces of the S3024 9,84% airfoil.

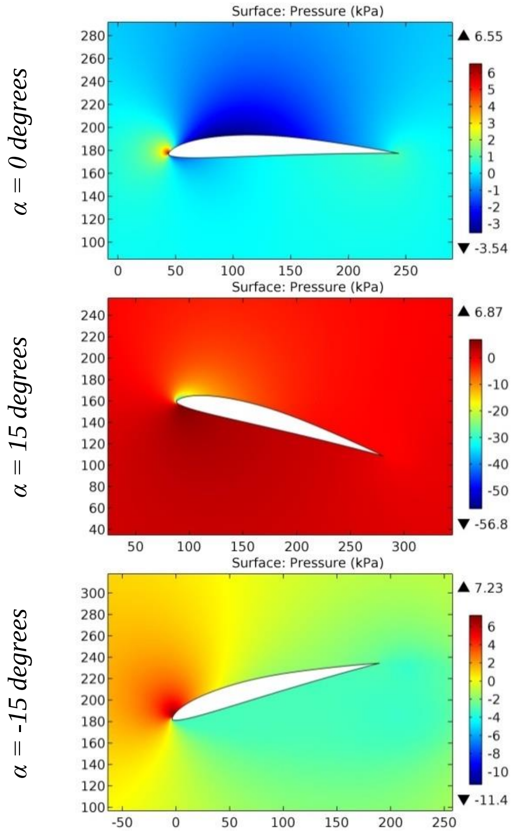

Figure 38. The pressure contours on the surfaces of the S3025 9,38% airfoil.

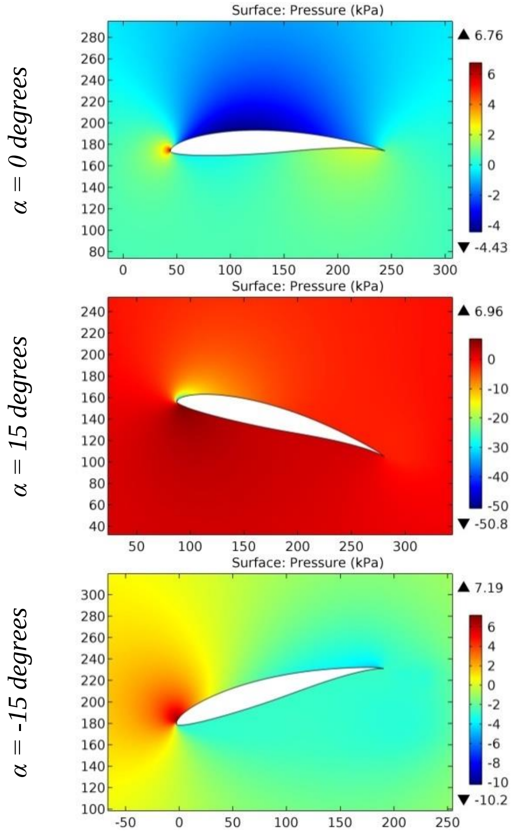

Figure 39. The pressure contours on the surfaces of the S4022 airfoil.

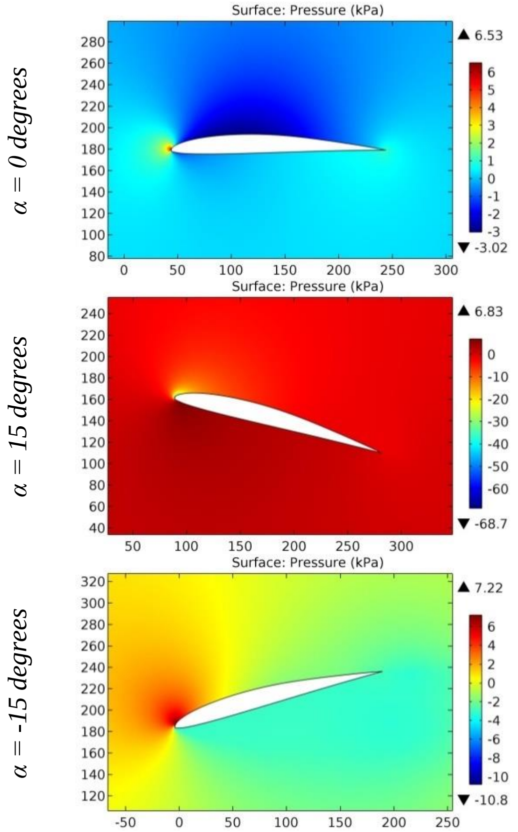

Figure 40. The pressure contours on the surfaces of the S4053 airfoil.

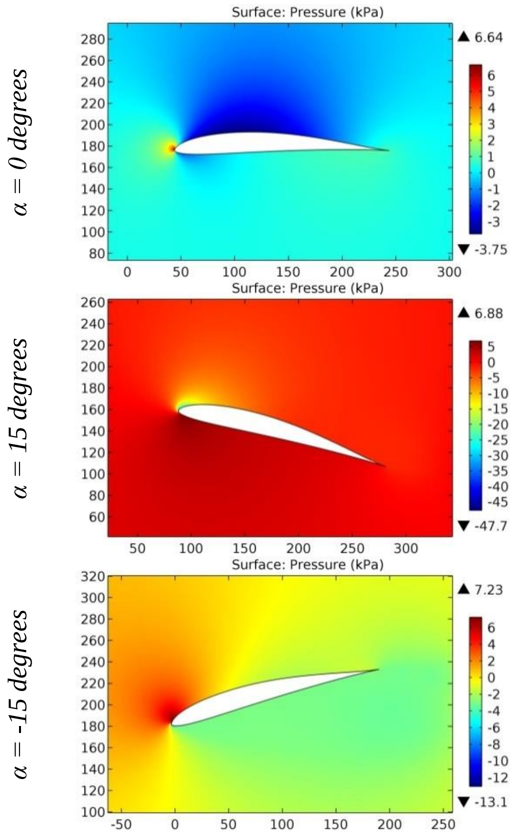

Figure 41. The pressure contours on the surfaces of the S4061 airfoil.

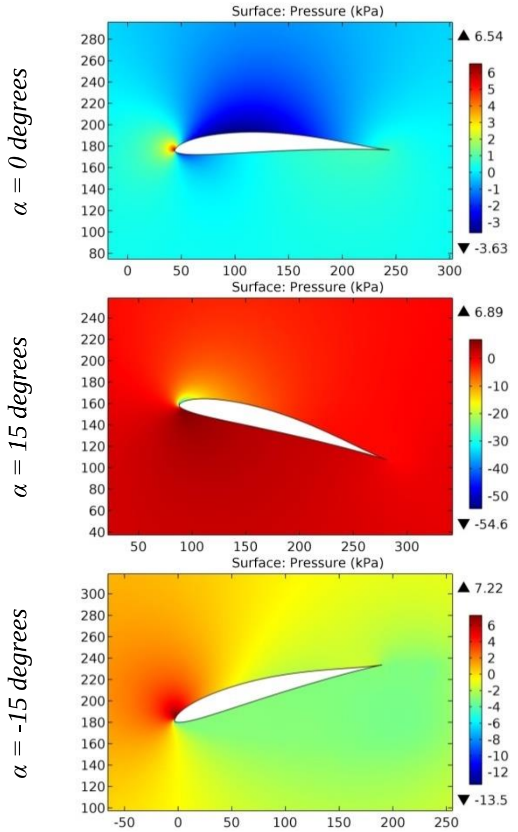

Figure 42. The pressure contours on the surfaces of the S4061-096-84 airfoil.

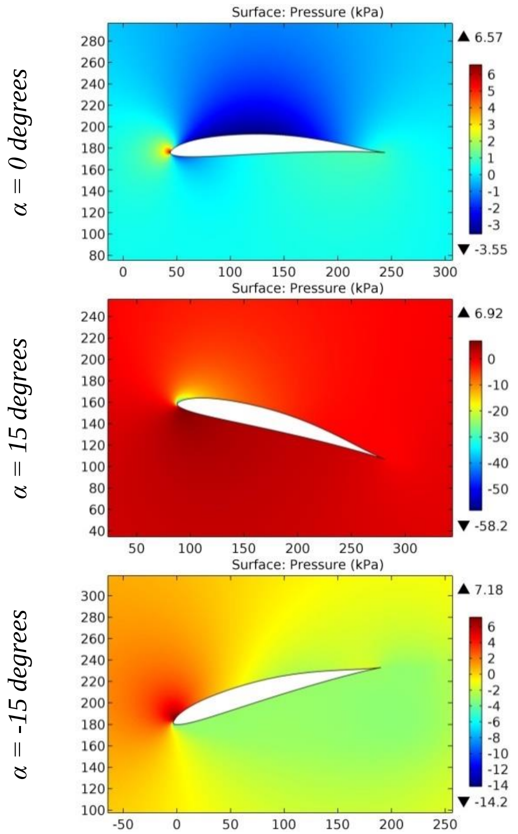

Figure 43. The pressure contours on the surfaces of the S4062 airfoil.

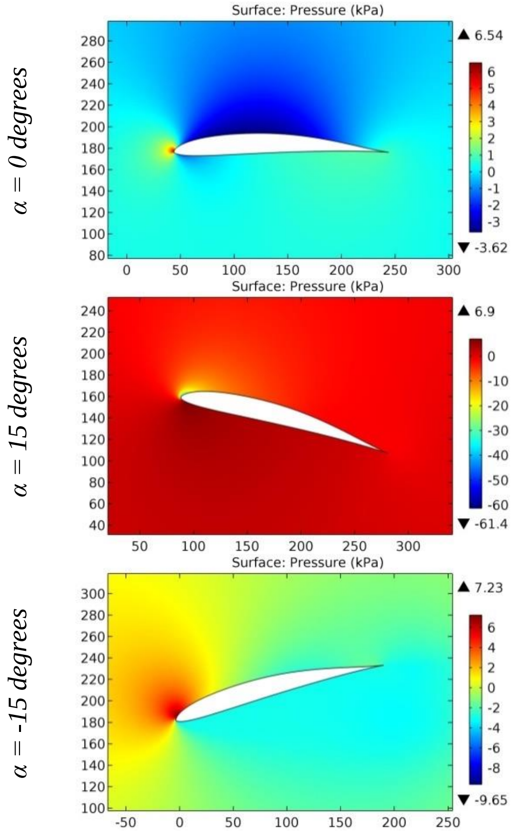

Figure 44. The pressure contours on the surfaces of the S4062-095-87 airfoil.

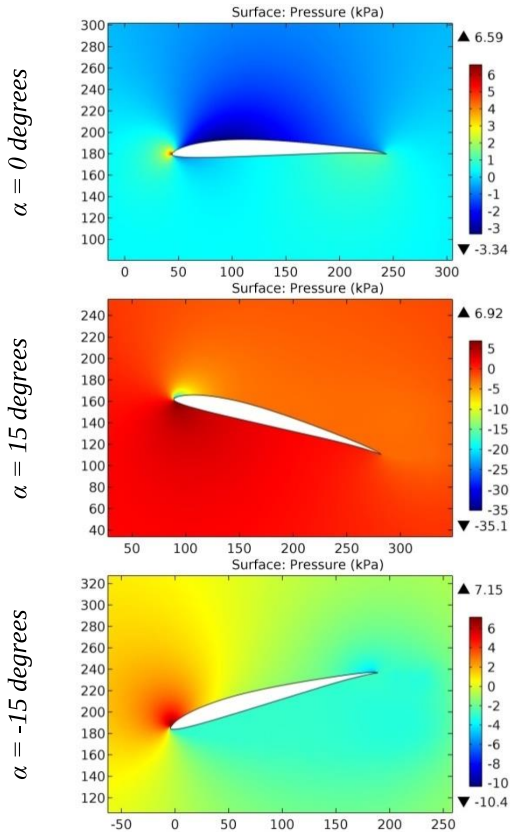

Figure 45. The pressure contours on the surfaces of the S4080 airfoil.

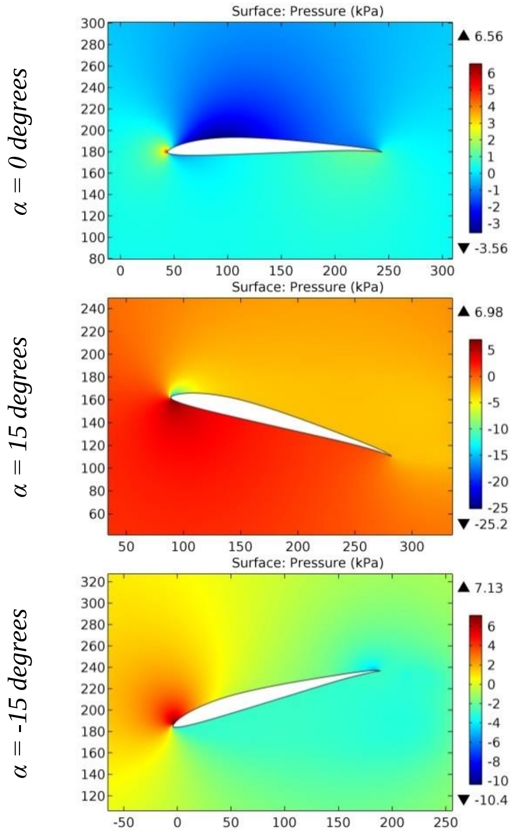

Figure 46. The pressure contours on the surfaces of the S4081 airfoil.

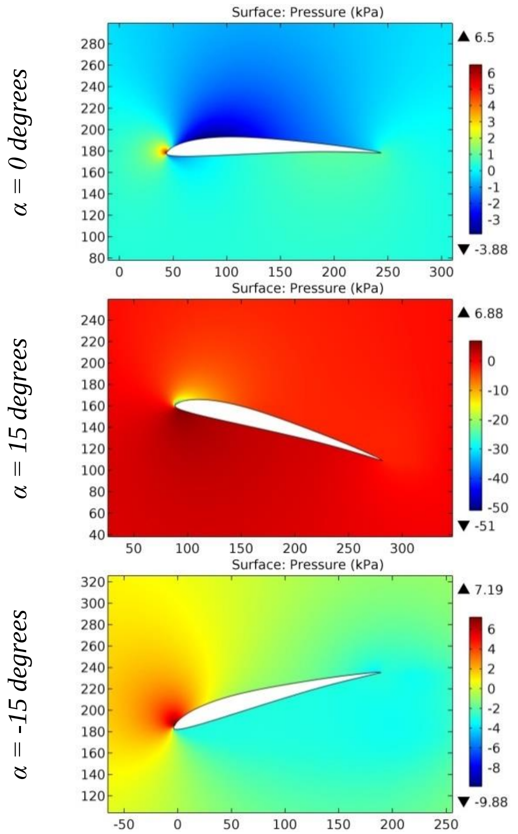

Figure 47. The pressure contours on the surfaces of the S4082 airfoil.

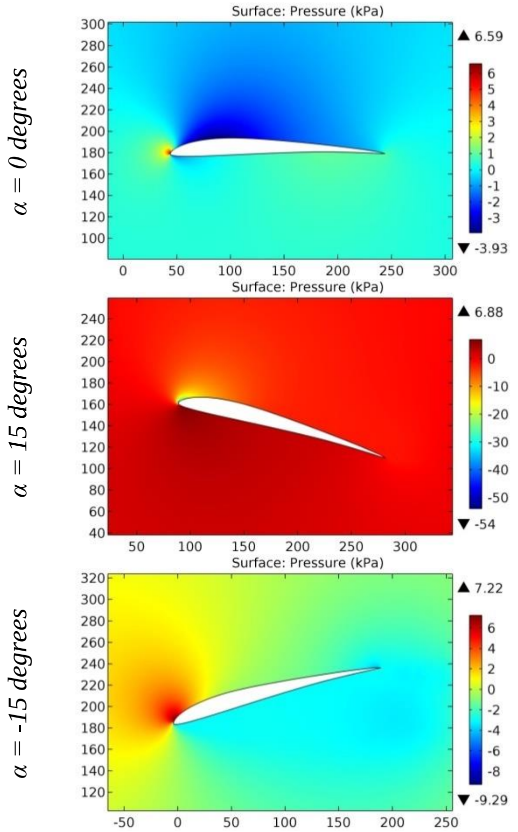

Figure 48. The pressure contours on the surfaces of the S4083 (8%) airfoil.

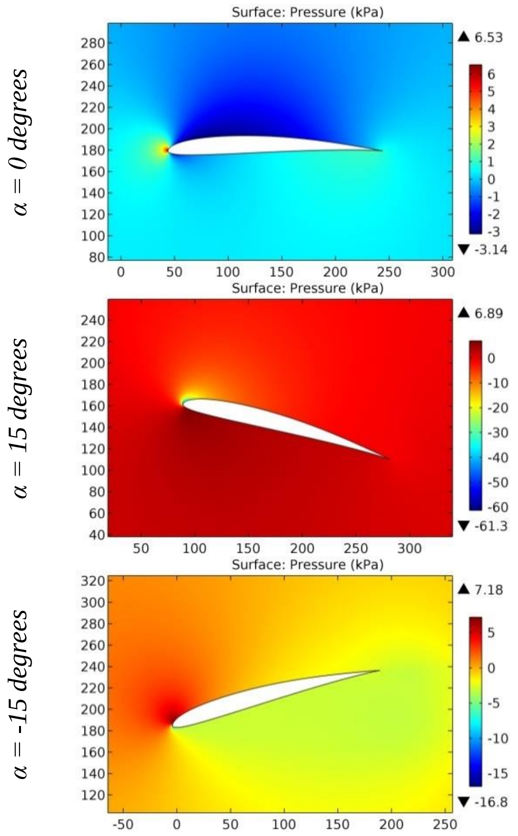

Figure 49. The pressure contours on the surfaces of the S4110 airfoil.

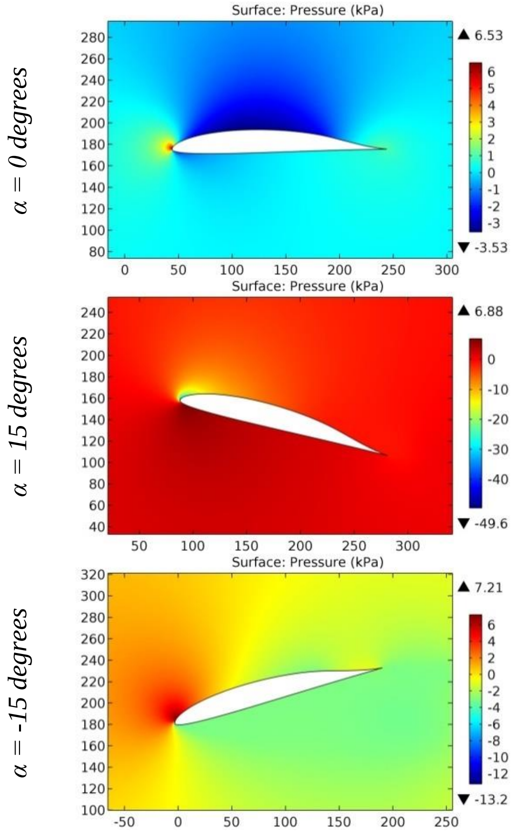

Figure 50. The pressure contours on the surfaces of the S4158 airfoil.

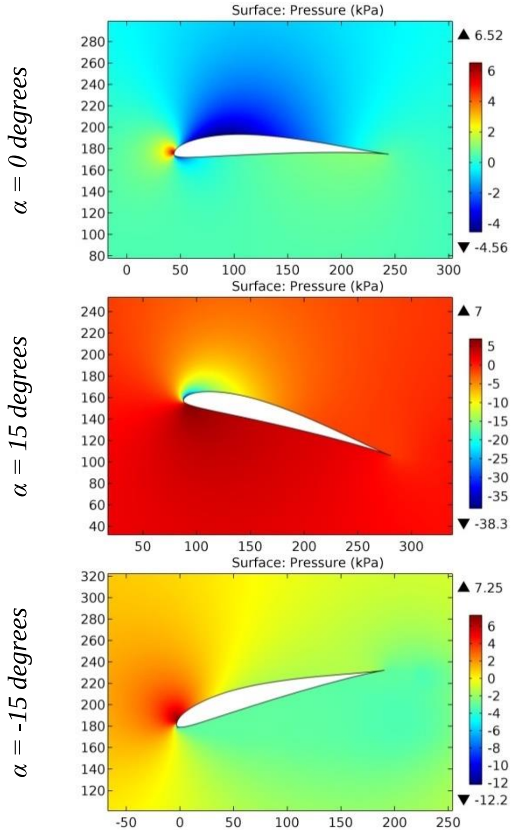

Figure 51. The pressure contours on the surfaces of the S4180 airfoil.

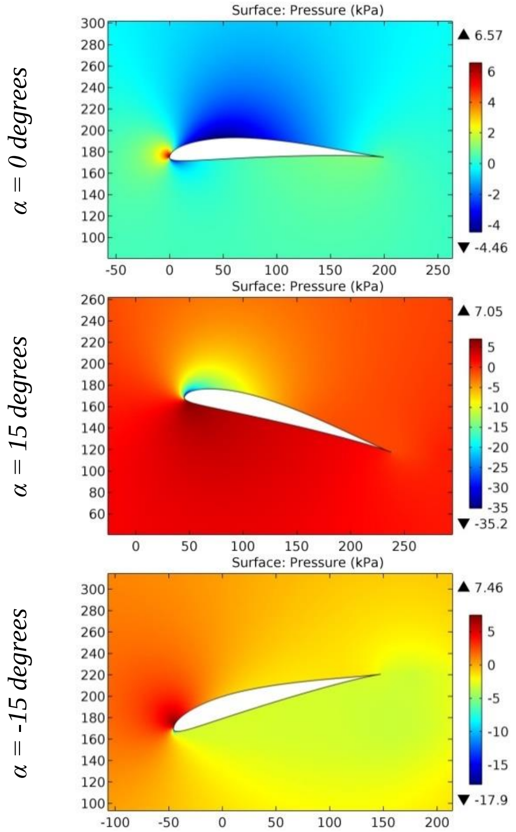

Figure 52. The pressure contours on the surfaces of the S4180-098-84 airfoil.

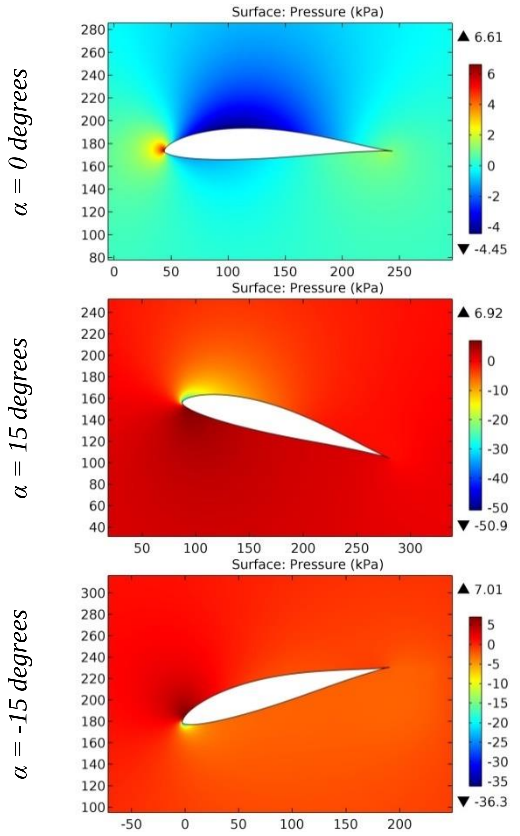

Figure 53. The pressure contours on the surfaces of the S4233 airfoil.

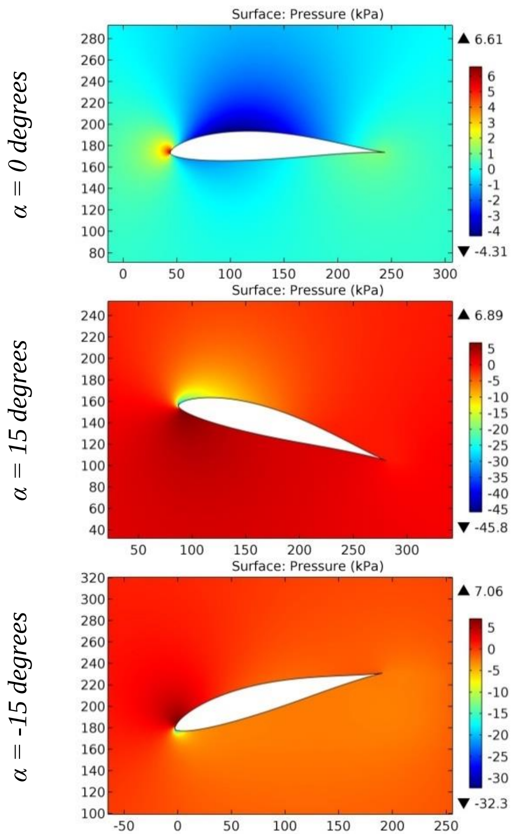

Figure 54. The pressure contours on the surfaces of the S4233-136-84 airfoil.

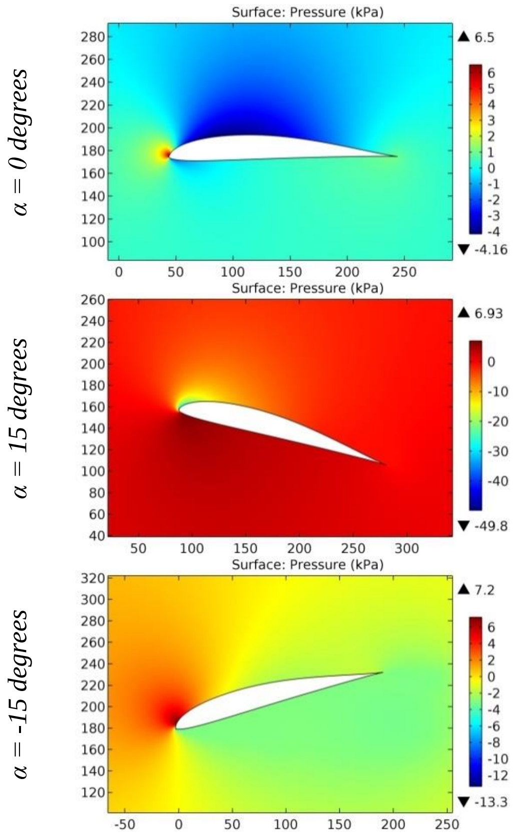

Figure 55. The pressure contours on the surfaces of the S4310 airfoil.

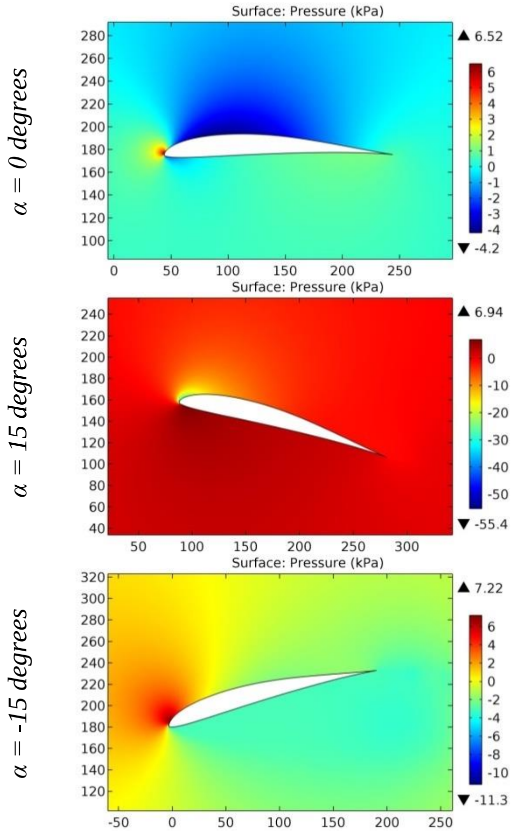

Figure 56. The pressure contours on the surfaces of the S4320 airfoil.

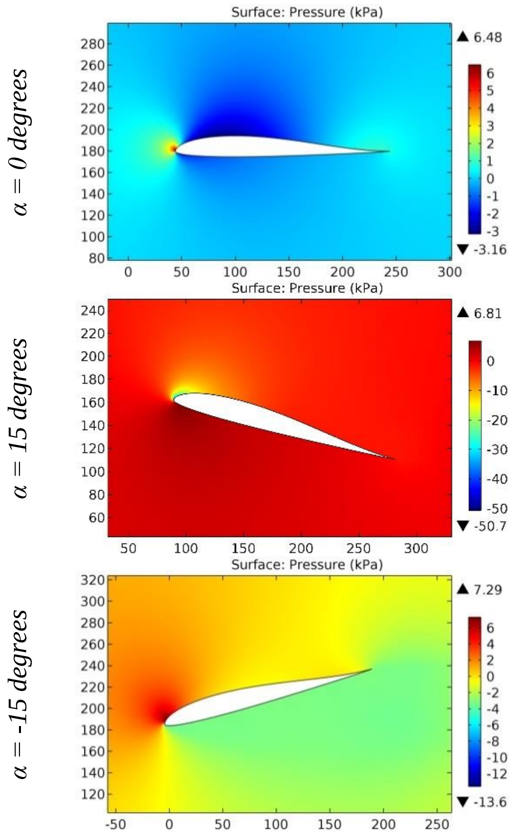

Figure 57. The pressure contours on the surfaces of the S5010 airfoil.

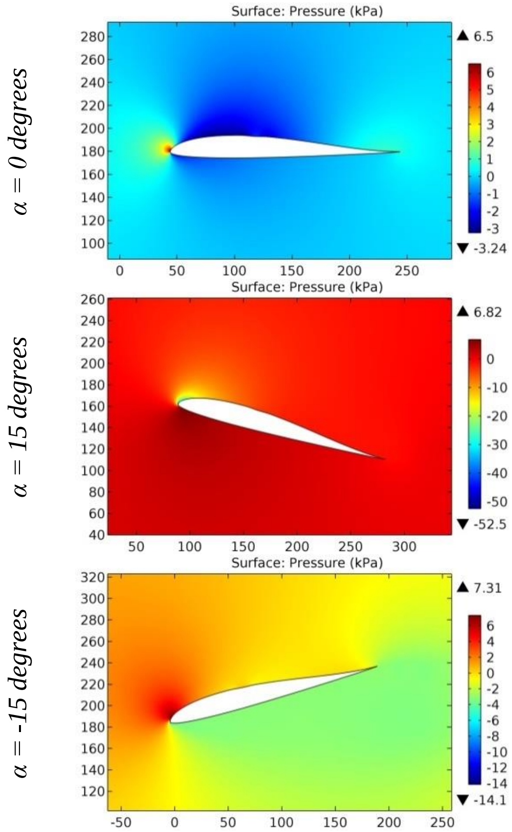

Figure 58. The pressure contours on the surfaces of the S5010-98 airfoil.

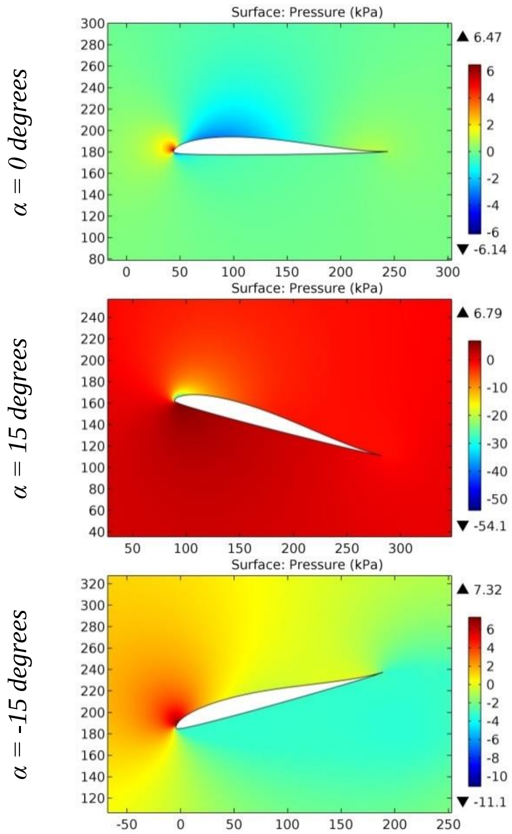

Figure 59. The pressure contours on the surfaces of the S5020 airfoil.

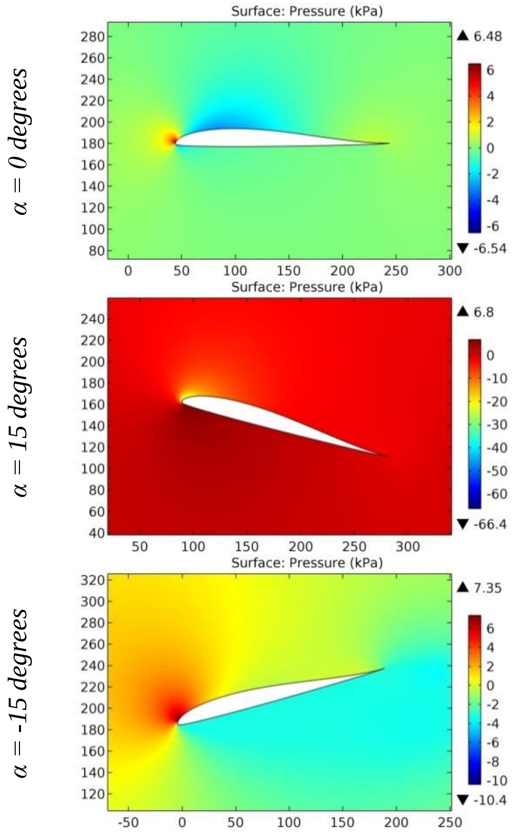

Figure 60. The pressure contours on the surfaces of the S5020-84 airfoil.

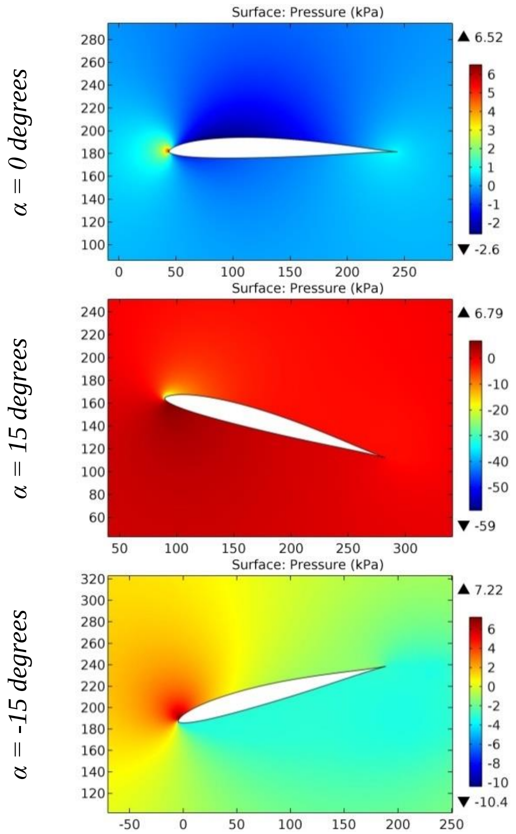

Figure 61. The pressure contours on the surfaces of the S6061 9% airfoil.

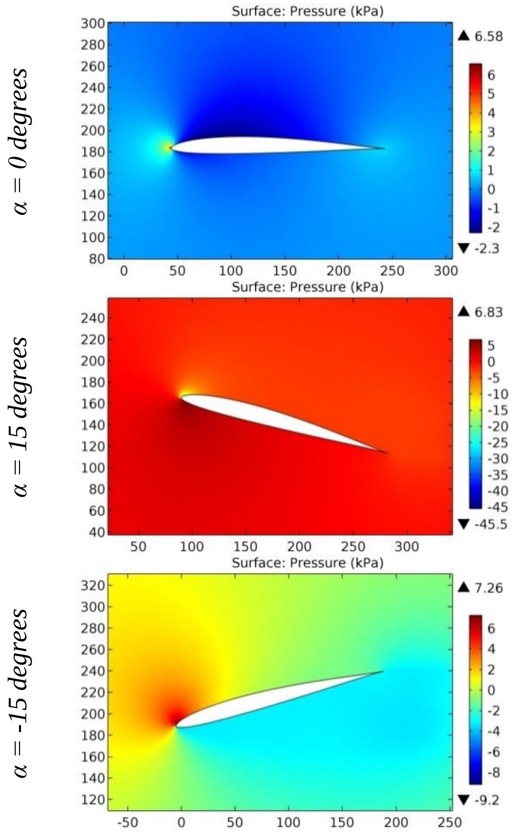

Figure 62. The pressure contours on the surfaces of the S6062 8% airfoil.

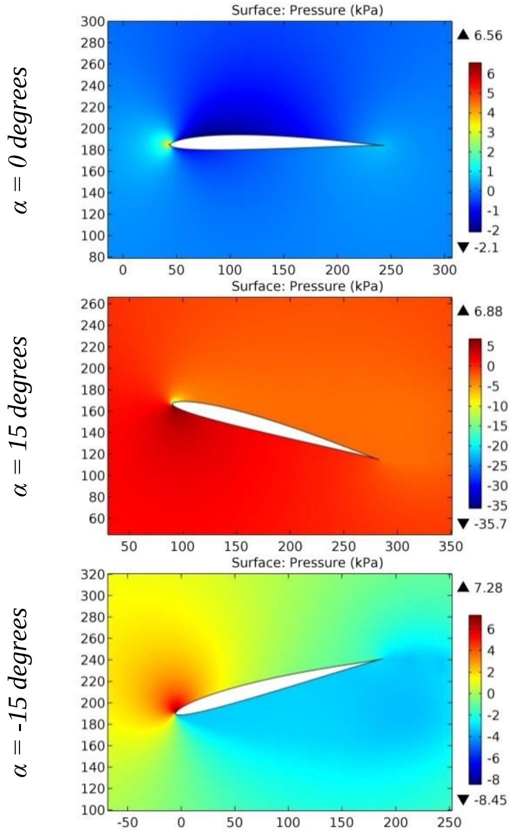

Figure 63. The pressure contours on the surfaces of the S6063 7,05% airfoil.

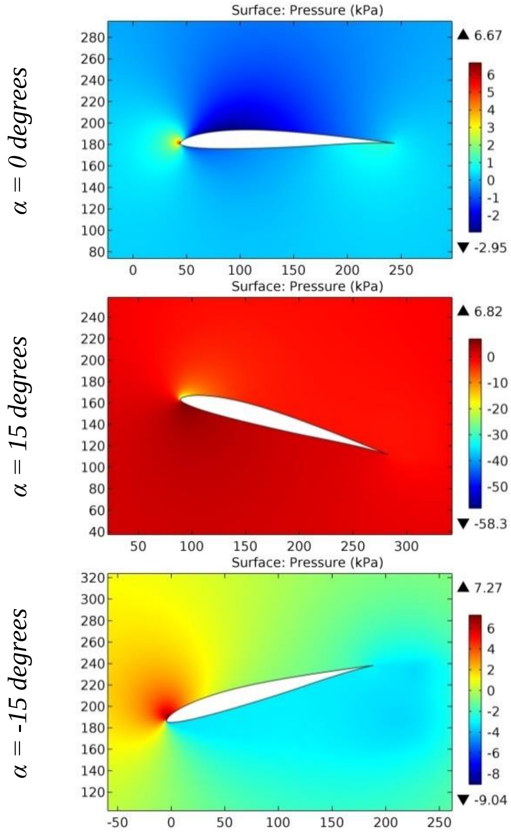

Figure 64. The pressure contours on the surfaces of the S7012 8,75% airfoil.

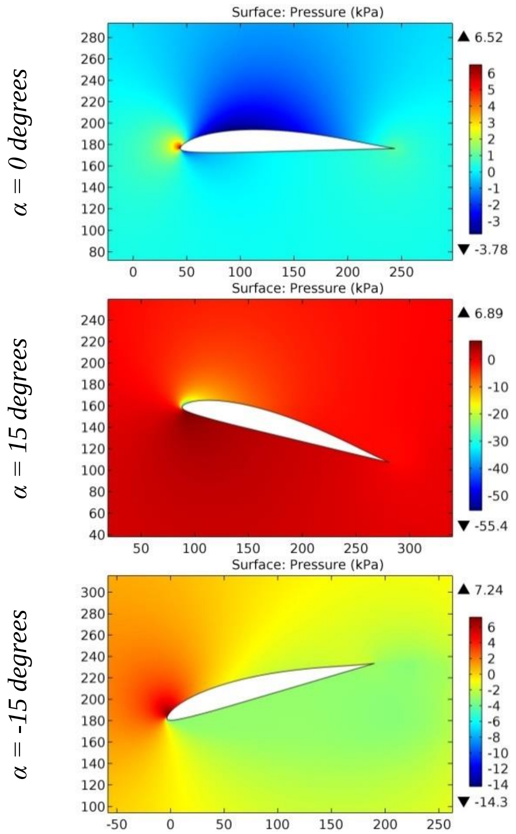

Figure 65. The pressure contours on the surfaces of the S7055 (10,5%) Flat-Bottomed airfoil.

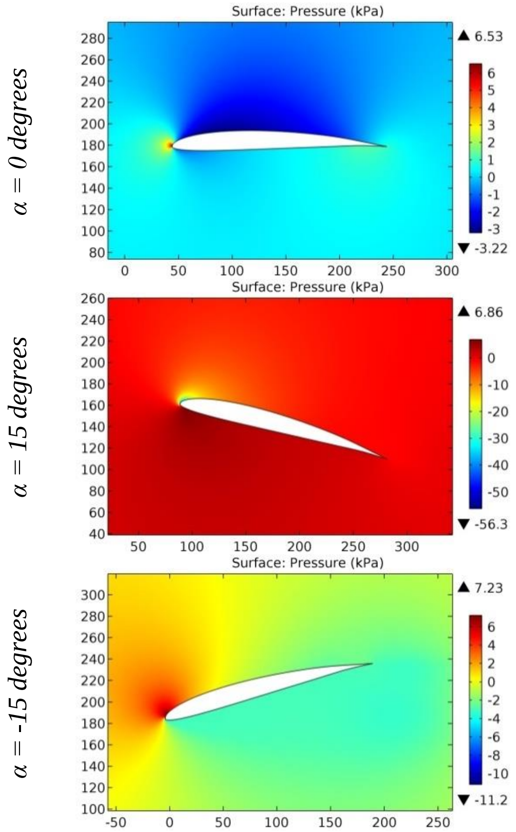

Figure 66. The pressure contours on the surfaces of the S7075 (9%) airfoil.

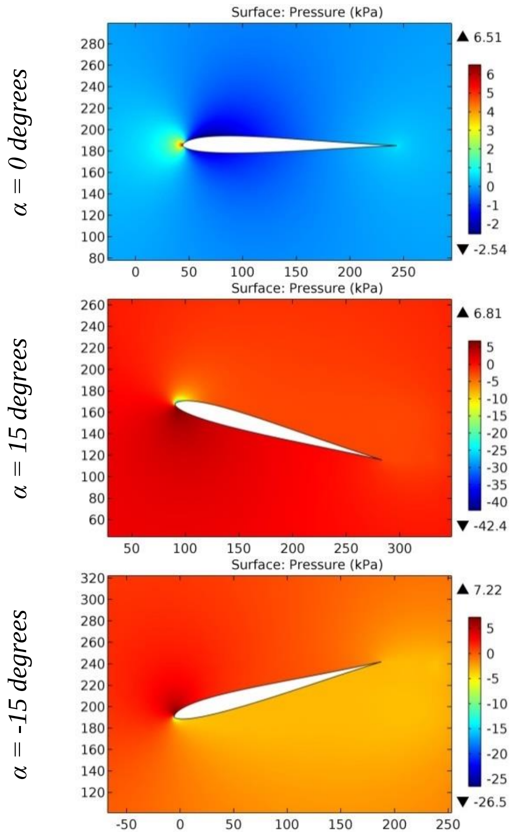

Figure 67. The pressure contours on the surfaces of the S8025 (8%) airfoil.

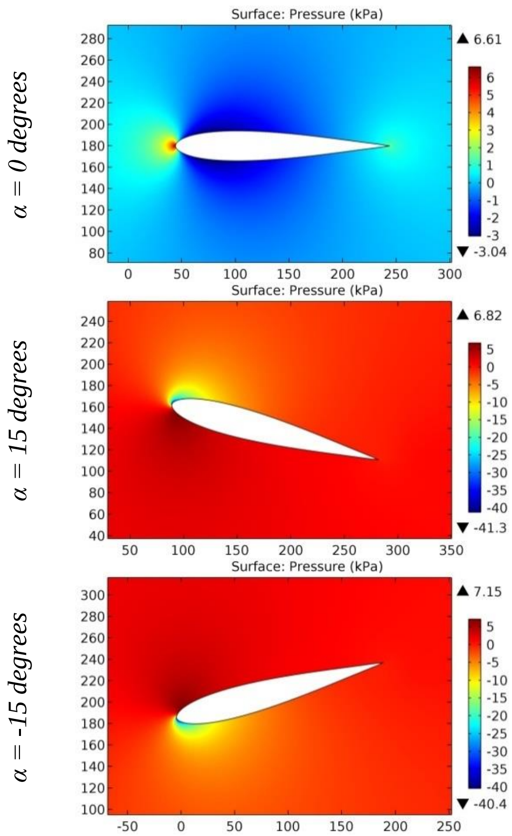

Figure 68. The pressure contours on the surfaces of the S8035 for RC aerobatic 14% thick airfoil.

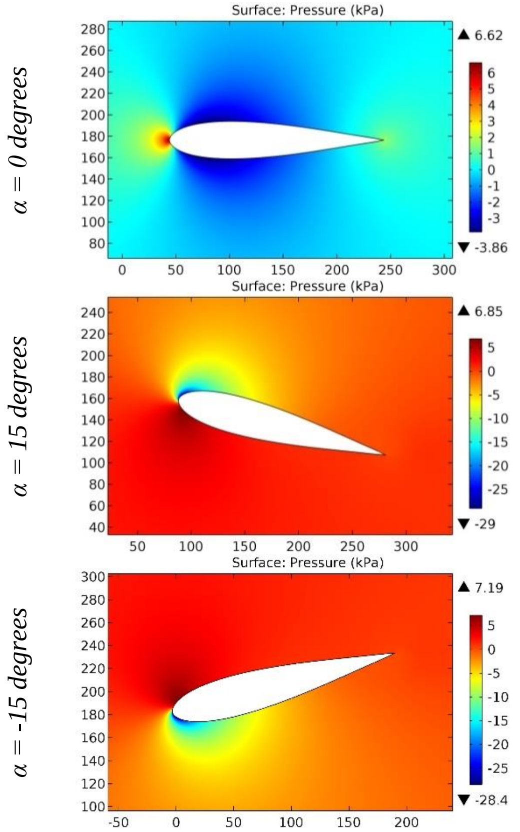

Figure 69. The pressure contours on the surfaces of the S8035-17,5% airfoil.

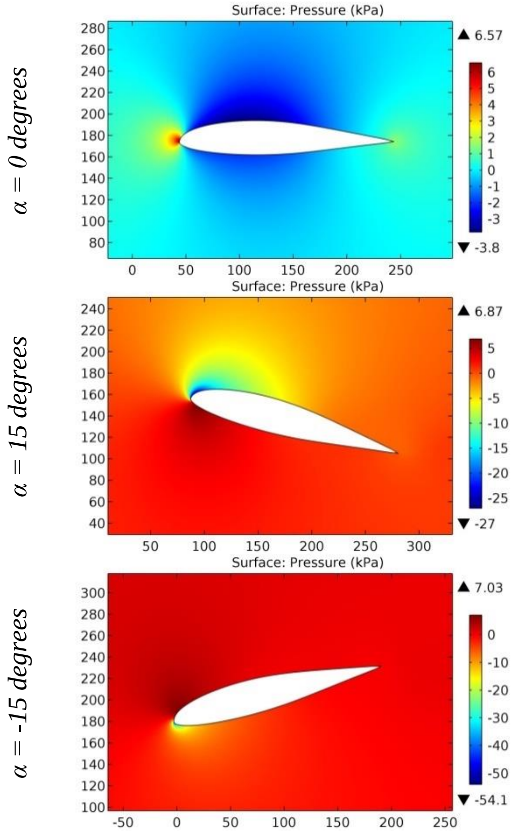

Figure 70. The pressure contours on the surfaces of the S8036 (16%) airfoil.

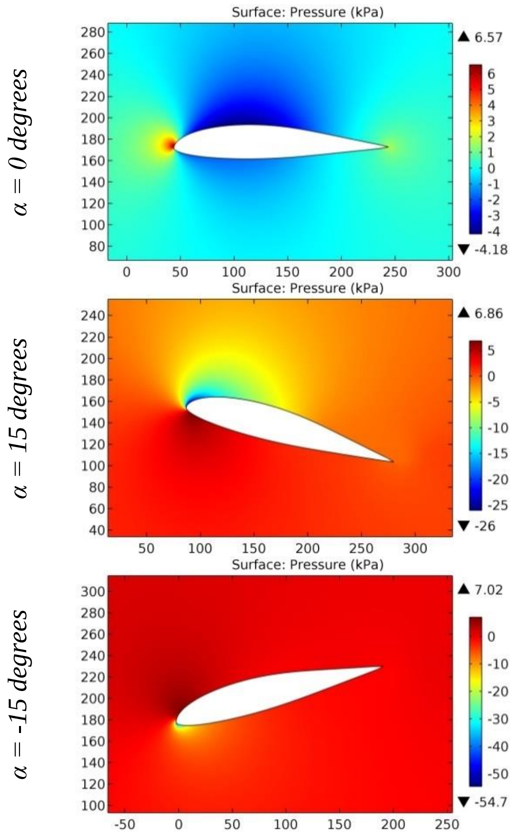

Figure 71. The pressure contours on the surfaces of the S8037 (16%) airfoil.

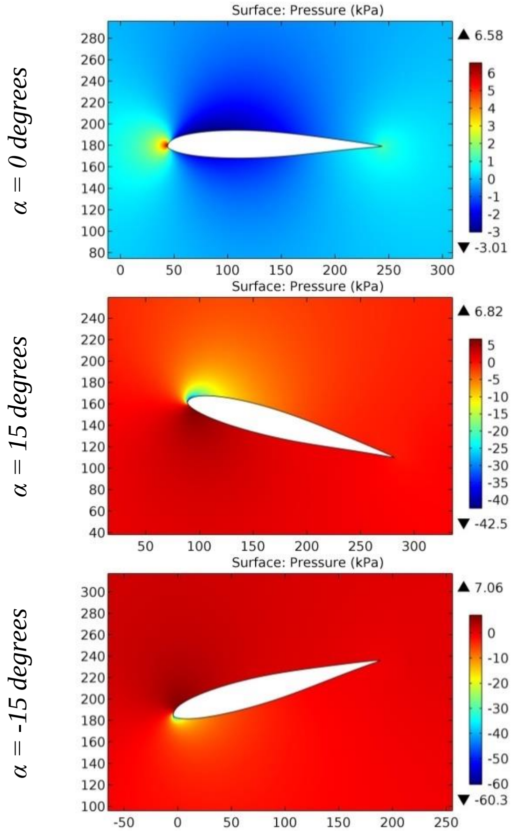

Figure 72. The pressure contours on the surfaces of the S8038 (13%) airfoil.

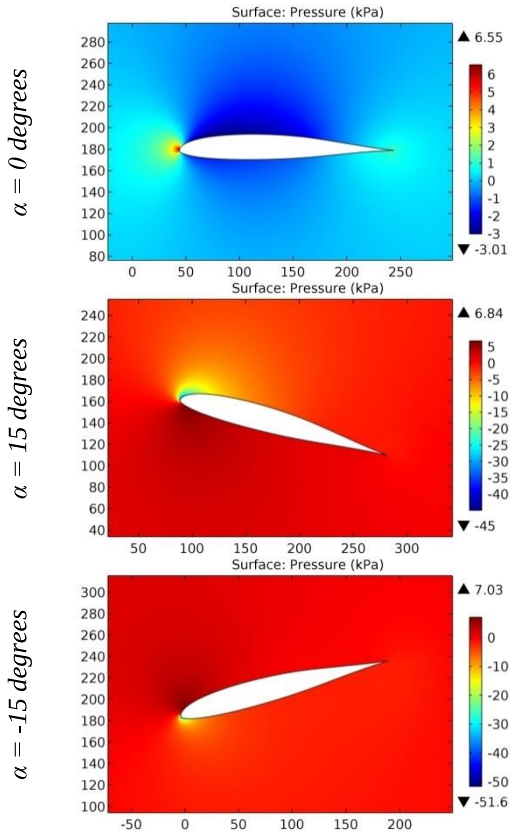

Figure 73. The pressure contours on the surfaces of the S8052 (11,88%) airfoil.

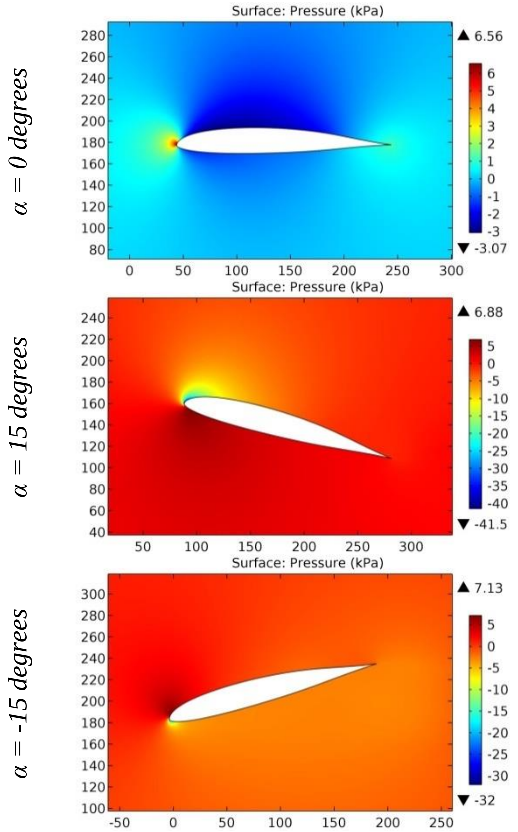

Figure 74. The pressure contours on the surfaces of the S8055 (12%) airfoil.

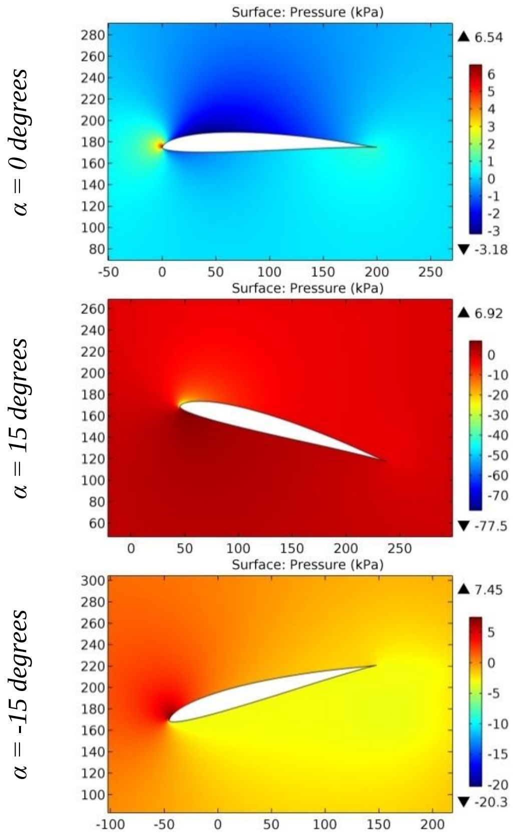

Figure 75. The pressure contours on the surfaces of the SA7035 airfoil.

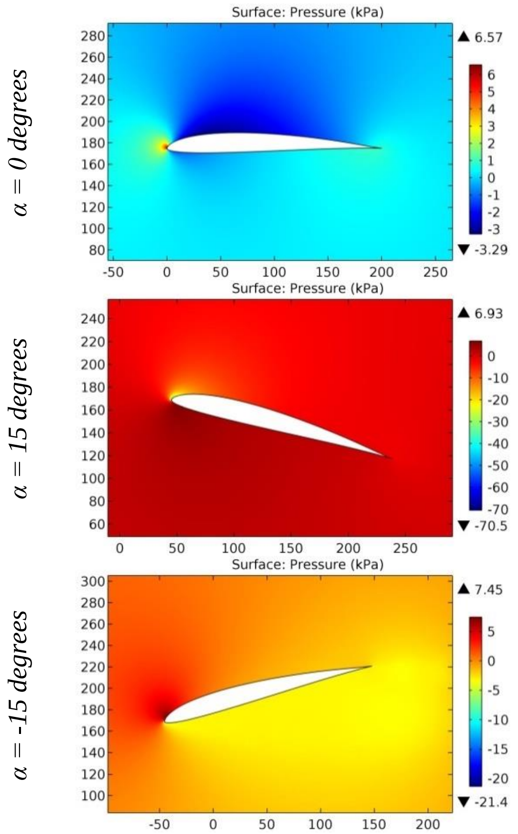

Figure 76. The pressure contours on the surfaces of the SA7036 airfoil.

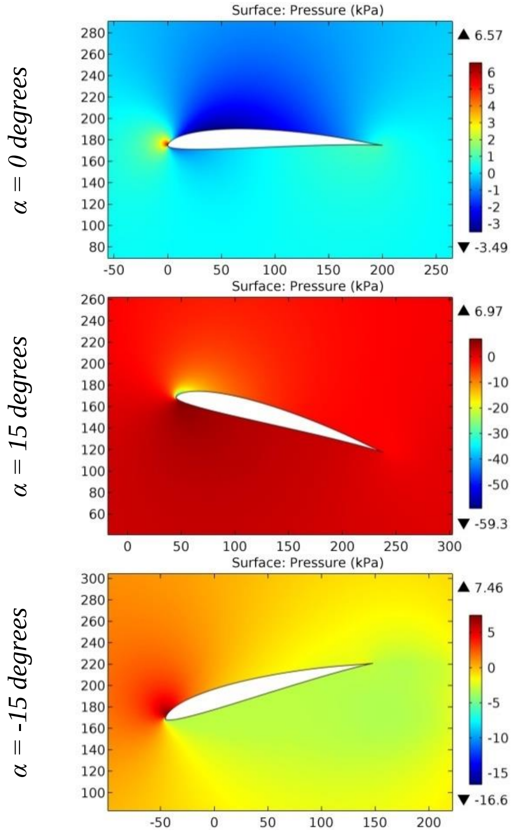

Figure 77. The pressure contours on the surfaces of the SA7038 airfoil.

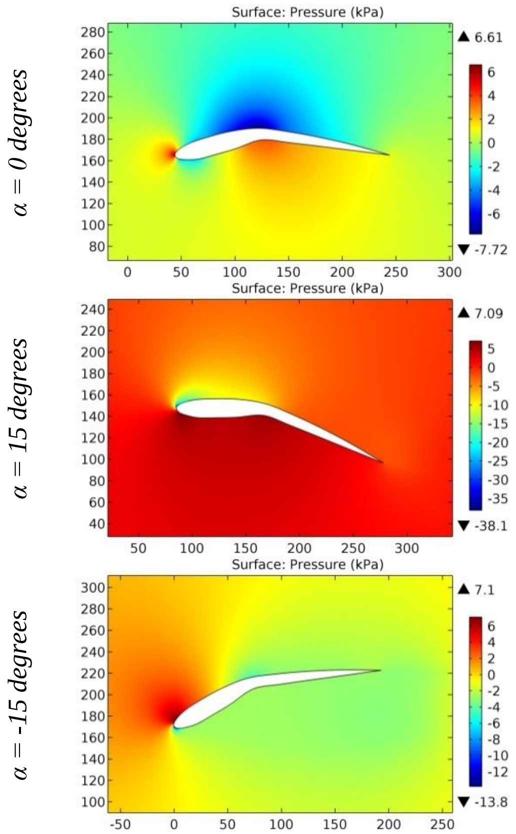

Figure 78. The pressure contours on the surfaces of the SARATOV airfoil.

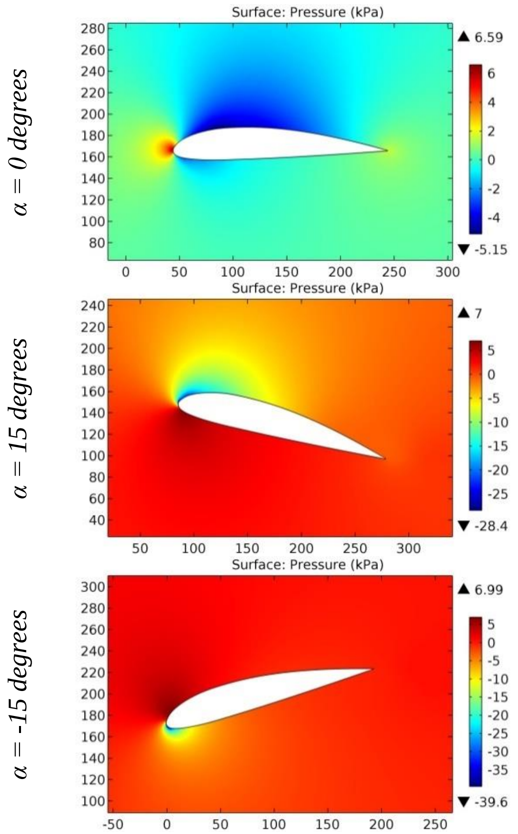

Figure 79. The pressure contours on the surfaces of the SAUTER1 airfoil.

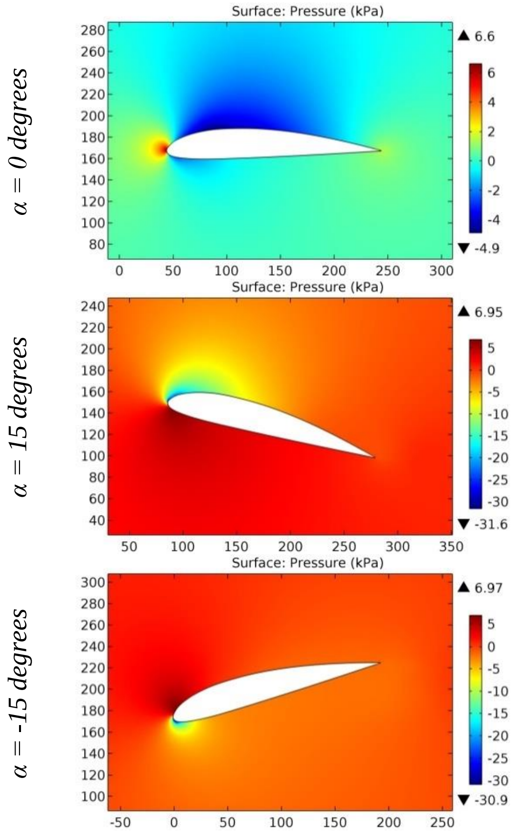

Figure 80. The pressure contours on the surfaces of the SAUTER2 airfoil.

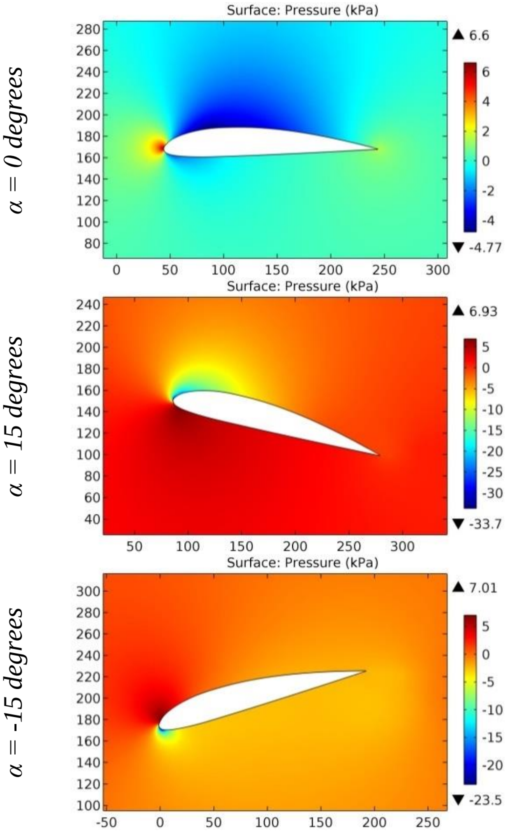

Figure 81. The pressure contours on the surfaces of the SAUTER3 airfoil.

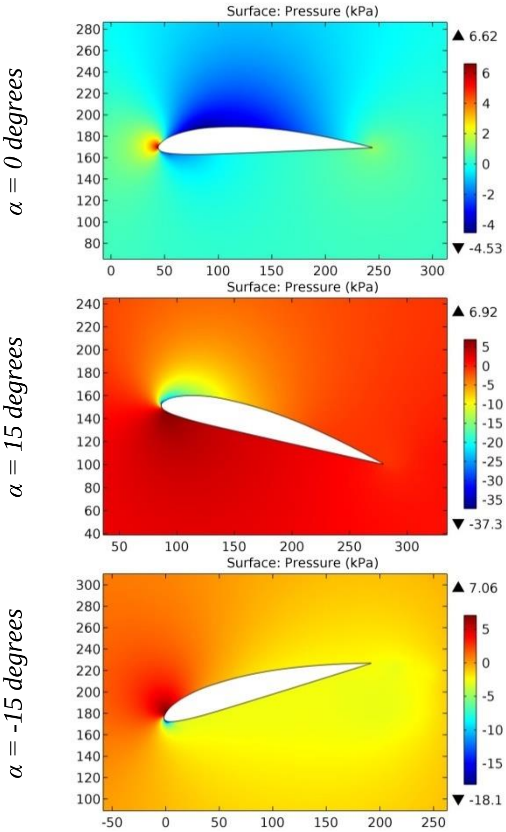

Figure 82. The pressure contours on the surfaces of the SAUTER4 airfoil.

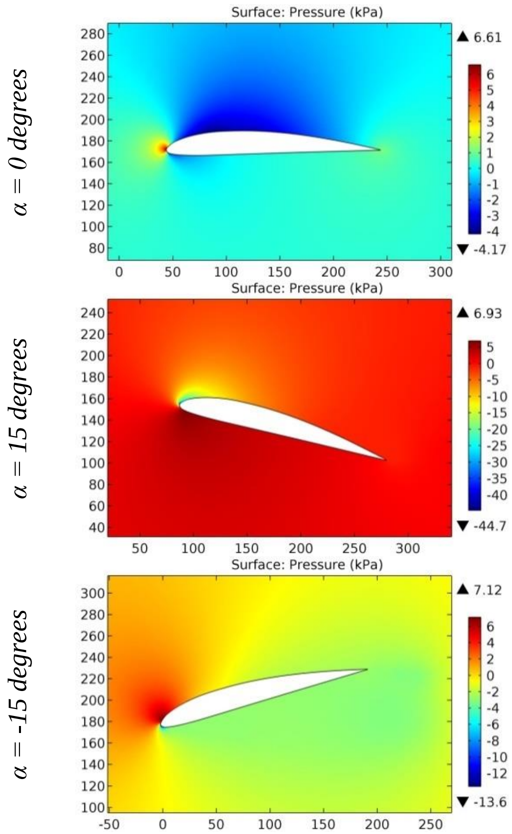

Figure 83. The pressure contours on the surfaces of the SAUTER5 airfoil.

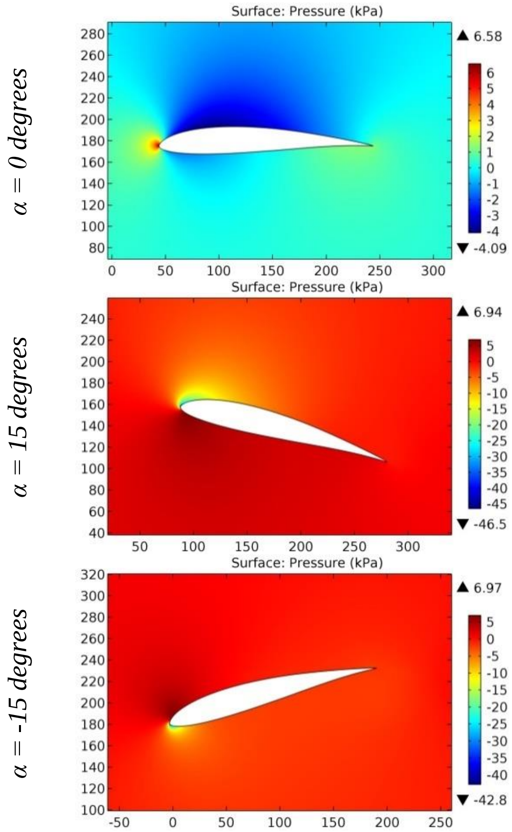

Figure 84. The pressure contours on the surfaces of the SB 96 12.7/3.0 airfoil.

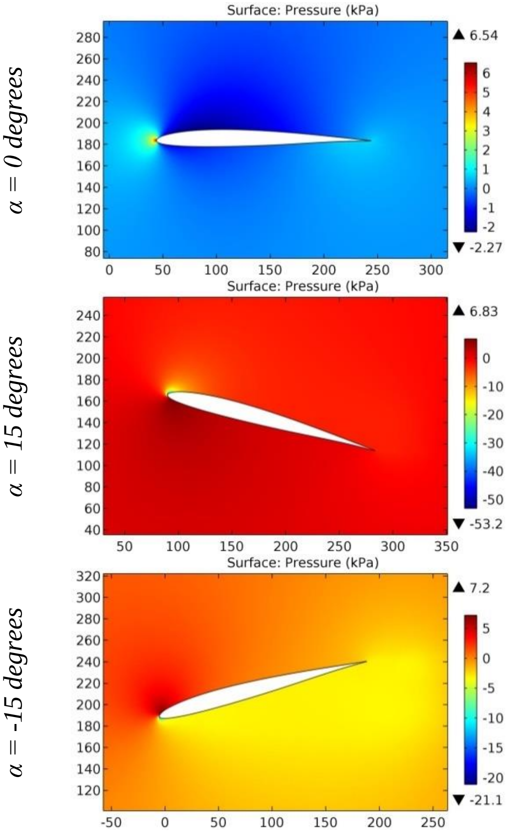

Figure 85. The pressure contours on the surfaces of the SB 97 8/1.25 airfoil.

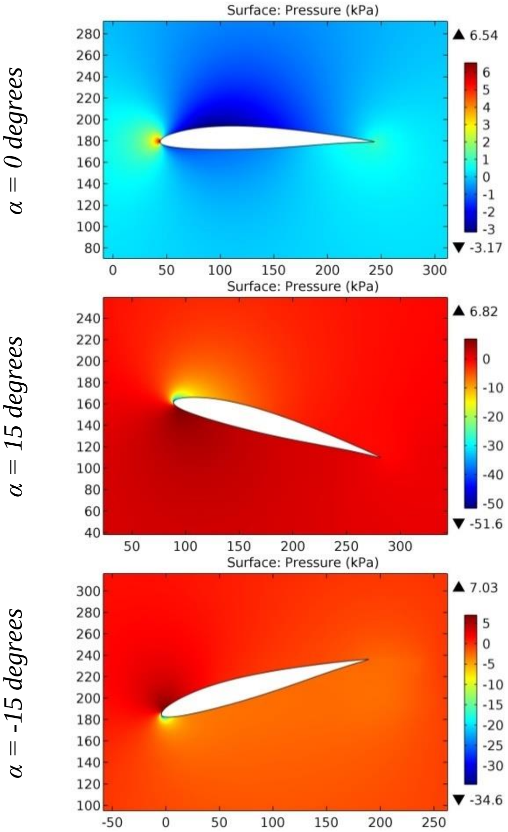

Figure 86. The pressure contours on the surfaces of the SB 98 VM5 airfoil.

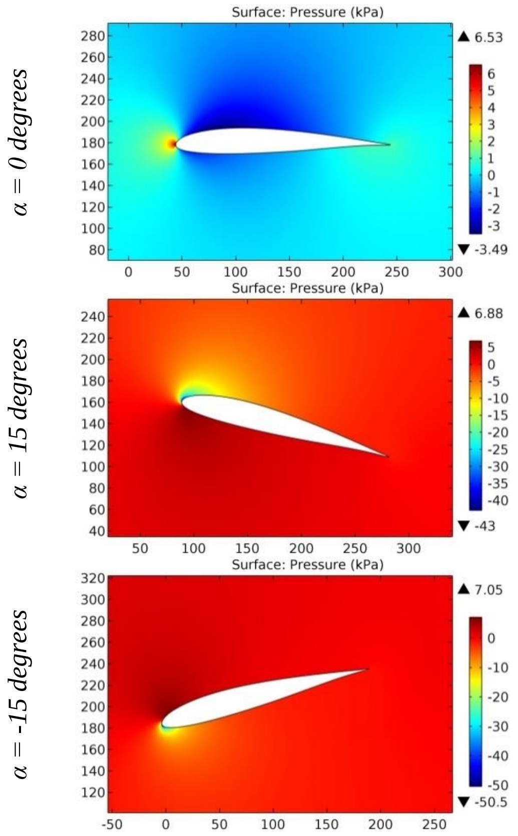

Figure 87. The pressure contours on the surfaces of the SB 98 VR5 airfoil.

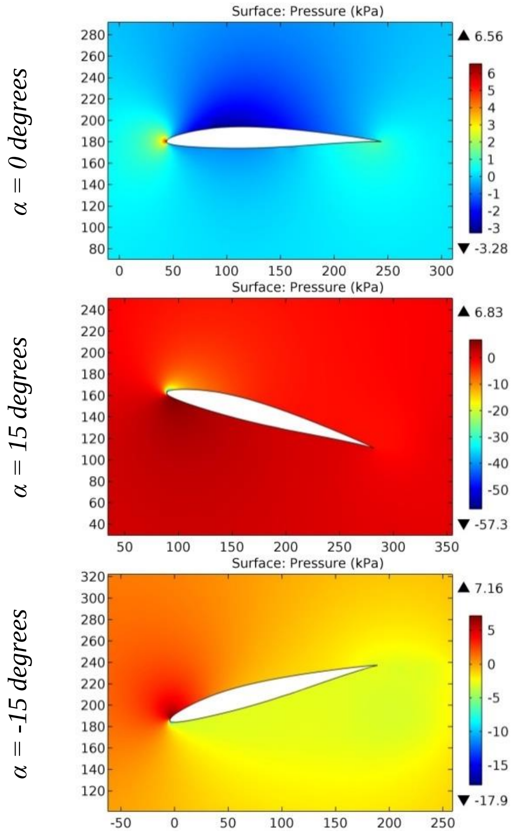

Figure 88. The pressure contours on the surfaces of the SB 98 VS5 airfoil.

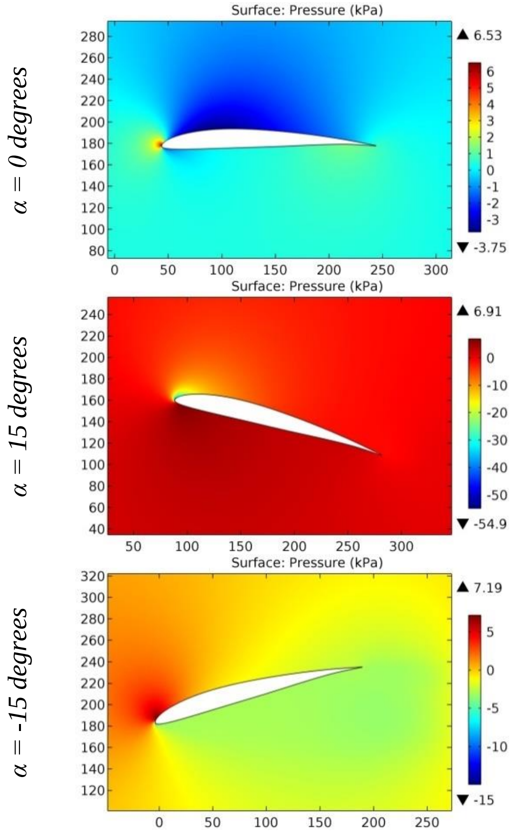

Figure 89. The pressure contours on the surfaces of the SB 99 F3J airfoil.

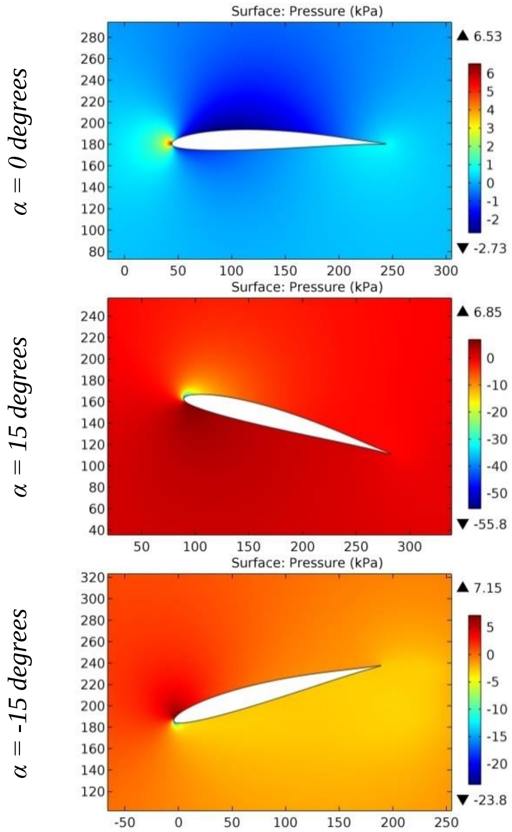

Figure 90. The pressure contours on the surfaces of the SB95 9.5/2 airfoil.

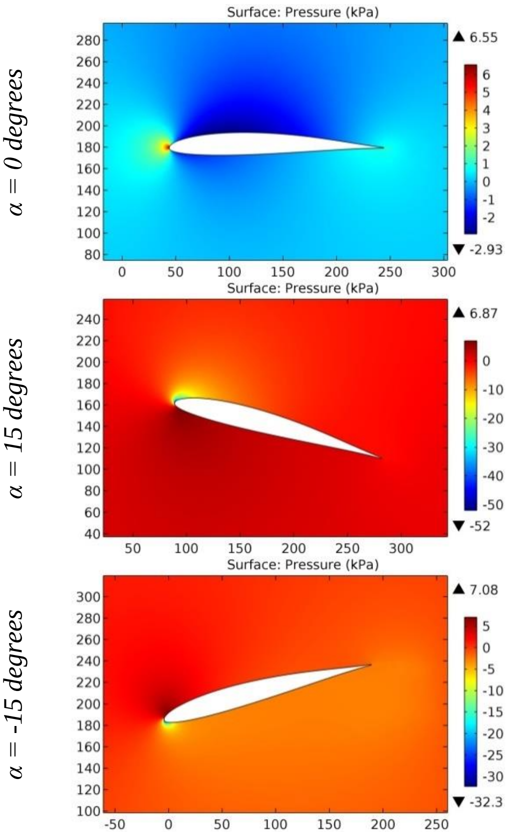

Figure 91. The pressure contours on the surfaces of the SB95 10.5/2 airfoil.

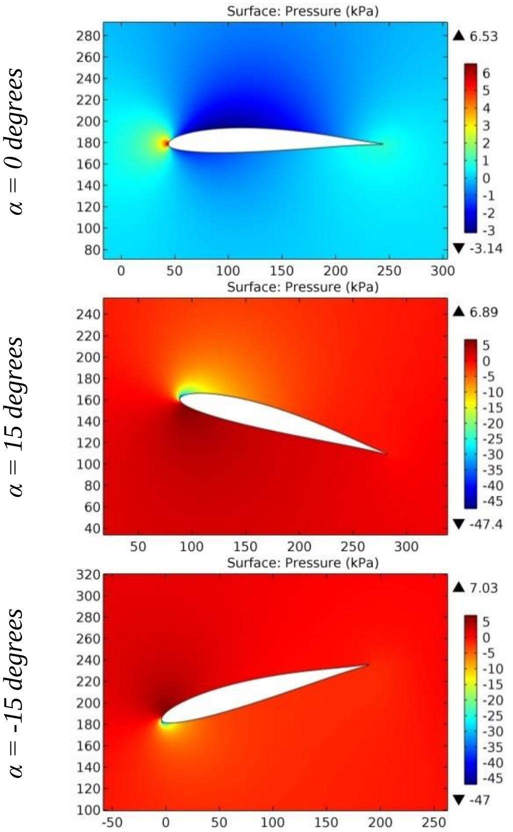

Figure 92. The pressure contours on the surfaces of the SB95 11.5/2 airfoil.

The convex upper surface of the S1020 airfoil ensures the formation of the greatest negative pressure gradient on it during the horizontal flight of the airplane. Under these conditions, the drag on the leading edge has an arithmetic mean calculated on the basis of the obtained pressure values. The wings experience more pressure on the frontal part during the airplane climb. The pressure drop is low.

The S1223 RTL airfoil is characterized by maxima of negative and positive pressures on the upper and lower surfaces. At the same time, the negative pressure is about 1.5 times greater than the positive pressure. This airfoil is subjected to greater negative pressure during the airplane climb. The pressure drop on the wing surfaces during the climb and descent of the airplane changes twice.

The calculated values of negative pressure on the surfaces of the S4158 airfoil during the airplane climb are 4 times greater than the values of negative pressure during the airplane descent. Negative pressure is formed at an angle of attack of +15 degrees on the leading edge, positive pressure is formed at an angle of attack of -15 degrees on the leading edge.

The analysis of the S7055 (10.5%) Flat-Bottomed airfoil showed a slight increase in negative pressure on the leading edge during the climb maneuver of the airplane. This conclusion was made when comparing this and the previous airfoils.

The teardrop shape of the S8035 for RC aerobatic 14% thick airfoil ensures the same distribution of the pressure gradient on the upper and lower surfaces. The drag on the leading edge is 2.18% higher during the airplane climb than during the descent.

The SARATOV curved airfoil is subjected to low variable pressures at selected angles of attack. Since this airfoil has a certain slope when horizontal flight of the airplane, the negative pressure on the surface will be higher than for other airfoils.

The SB 98 VS5 airfoil is subjected to higher pressure on the frontal part compared to other airfoils considered in detail during the airplane climb. Pressure varies from minimum to maximum values by almost 9 times.

Conclusion

Simulation of the air flow around the airplane wings allows you to obtain calculated values of effective pressure, flow velocity and other parameters at different angles of attack. Thus, it is possible to choose the configuration of the airfoil for specific flight conditions of the airplane. The created database of aerodynamic characteristics of the airfoils will be the basis for the projected wing of the airplane, which will have the most optimal geometry.

References:

1. Anderson, J. D. (2010). *Fundamentals of Aerodynamics.* McGraw-Hill, Fifth edition.
2. Shevell, R. S. (1989). *Fundamentals of Flight.* Prentice Hall, Second edition.
3. Houghton, E. L., & Carpenter, P. W. (2003). *Aerodynamics for Engineering Students*. Fifth edition, Elsevier.
4. Lan, E. C. T., & Roskam, J. (2003). *Airplane Aerodynamics and Performance.* DAR Corp.
5. Sadraey, M. (2009). *Aircraft Performance Analysis.* VDM Verlag Dr. Müller.
6. Anderson, J. D. (1999). *Aircraft Performance and Design*. McGraw-Hill.
7. Roskam, J. (2007). *Airplane Flight Dynamics and Automatic Flight Control*, Part I. DAR Corp.
8. Etkin, B., & Reid, L. D. (1996). *Dynamics of Flight, Stability and Control.* Third Edition, Wiley.
9. Stevens, B. L., & Lewis, F. L. (2003). *Aircraft Control and Simulation.* Second Edition, Wiley.
10. Chemezov, D., et al. (2021). Pressure distribution on the surfaces of the NACA 0012 airfoil under conditions of changing the angle of attack. *ISJ Theoretical & Applied Science, 09 (101)*, 601-606.
11. Chemezov, D., et al. (2021). Stressed state of surfaces of the NACA 0012 airfoil at high angles of attack. *ISJ Theoretical & Applied Science, 10 (102)*, 601-604.
12. Chemezov, D., et al. (2021). Reference data of pressure distribution on the surfaces of airfoils having the names beginning with the letter A (the first part). *ISJ Theoretical & Applied Science, 10 (102)*, 943-958.
13. Chemezov, D., et al. (2021). Reference data of pressure distribution on the surfaces of airfoils having the names beginning with the letter A (the second part). *ISJ Theoretical & Applied Science, 11 (103)*, 656-675.
14. Chemezov, D., et al. (2021). Reference data of pressure distribution on the surfaces of airfoils having the names beginning with the letter B. *ISJ Theoretical & Applied Science, 11 (103)*, 1001-1076.
15. Chemezov, D., et al. (2021). Reference data of pressure distribution on the surfaces of airfoils

having the names beginning with the letter C. *ISJ Theoretical & Applied Science, 12 (104)*, 814-844.
16. Chemezov, D., et al. (2021). Reference data of pressure distribution on the surfaces of airfoils having the names beginning with the letter D. *ISJ Theoretical & Applied Science, 12 (104)*, 1244-1274.
17. Chemezov, D., et al. (2022). Reference data of pressure distribution on the surfaces of airfoils (hydrofoils) having the names beginning with the letter E (the first part). *ISJ Theoretical & Applied Science, 01 (105)*, 501-569.
18. Chemezov, D., et al. (2022). Reference data of pressure distribution on the surfaces of airfoils (hydrofoils) having the names beginning with the letter E (the second part). *ISJ Theoretical & Applied Science, 01 (105)*, 601-671.
19. Chemezov, D., et al. (2022). Reference data of pressure distribution on the surfaces of airfoils having the names beginning with the letter F. *ISJ Theoretical & Applied Science, 02 (106)*, 101-135.
20. Chemezov, D., et al. (2022). Reference data of pressure distribution on the surfaces of airfoils having the names beginning with the letter G (the first part). *ISJ Theoretical & Applied Science, 03 (107)*, 701-784.
21. Chemezov, D., et al. (2022). Reference data of pressure distribution on the surfaces of airfoils having the names beginning with the letter G (the second part). *ISJ Theoretical & Applied Science, 03 (107)*, 901-984.
22. Chemezov, D., et al. (2022). Reference data of pressure distribution on the surfaces of airfoils having the names beginning with the letter G (the third part). *ISJ Theoretical & Applied Science, 04 (108)*, 401-484.
23. Chemezov, D., et al. (2022). Reference data of pressure distribution on the surfaces of airfoils having the names beginning with the letter H (the first part). *ISJ Theoretical & Applied Science, 05 (109)*, 201-258.
24. Chemezov, D., et al. (2022). Reference data of pressure distribution on the surfaces of airfoils having the names beginning with the letter H (the second part). *ISJ Theoretical & Applied Science, 05 (109)*, 529-586.
25. Chemezov, D., et al. (2022). Reference data of pressure distribution on the surfaces of airfoils having the names beginning with the letter I. *ISJ Theoretical & Applied Science, 06 (110)*, 1-7.
26. Chemezov, D., et al. (2022). Reference data of pressure distribution on the surfaces of airfoils having the names beginning with the letter J. *ISJ Theoretical & Applied Science, 06 (110)*, 18-25.
27. Chemezov, D., et al. (2022). Reference data of pressure distribution on the surfaces of airfoils having the names beginning with the letter K. *ISJ Theoretical & Applied Science, 07 (111)*, 1-10.
28. Chemezov, D., et al. (2022). Reference data of pressure distribution on the surfaces of airfoils having the names beginning with the letter L. *ISJ Theoretical & Applied Science, 07 (111)*, 101-118.
29. Chemezov, D., et al. (2022). Reference data of pressure distribution on the surfaces of airfoils having the names beginning with the letter M. *ISJ Theoretical & Applied Science, 10 (114)*, 307-392.
30. Chemezov, D., et al. (2022). Reference data of pressure distribution on the surfaces of airfoils having the names beginning with the letter N (the first part). *ISJ Theoretical & Applied Science, 12 (116)*, 801-892.
31. Chemezov, D., et al. (2022). Reference data of pressure distribution on the surfaces of airfoils having the names beginning with the letter N (the second part). *ISJ Theoretical & Applied Science, 12 (116)*, 901-990.
32. Chemezov, D., et al. (2023). Reference data of pressure distribution on the surfaces of airfoils having the names beginning with the letter O. *ISJ Theoretical & Applied Science, 01 (117)*, 624-635.
33. Chemezov, D., et al. (2023). Reference data of pressure distribution on the surfaces of airfoils having the names beginning with the letter P. *ISJ Theoretical & Applied Science, 02 (118)*, 48-61.
34. Chemezov, D., et al. (2023). Reference data of pressure distribution on the surfaces of airfoils having the names beginning with the letter R. *ISJ Theoretical & Applied Science, 03 (119)*, 104-165.